Modelling of flow, heat and thermal deformations to understand and optimize the performance of a hot air side sealer machine

Mikael Karlsson

DIVISION OF INNOVATION | DEPARTMENT OF DESIGN SCIENCES
FACULTY OF ENGINEERING LTH | LUND UNIVERSITY
2026

MASTER THESIS

Modelling of flow, heat and thermal deformations to understand and optimize the performance of a hot air side sealer machine

Mikael Karlsson

Lund University

Modelling of flow, heat and thermal deformations to understand and optimize the performance of a hot air side sealer machine

Published by
Department of Design Sciences
Faculty of Engineering LTH, Lund University
P.O. Box 118, SE-221 00 Lund, Sweden

Subject: Product Development (MMKM05)
Division: Division of Innovation, Department of Design Sciences, Faculty of Engineering LTH, Lund university
Supervisor: Axel Nordin
Co-supervisor: Lars Palm
Supervisors at Tetra Pak: Dr. Aurelia Vallier and Johan Nordgren
Examiner: Joze Tavcar

Abstract

In this master's thesis work, numerical simulation tools - computational fluid dynamics (CFD) and finite element method (FEM) - are used to predict the flow, the temperature field and the deformations within a machine for sealing the vertical seam of a carton package. The blank - the packaging material folded as a U-shape - is fed into the machine - the side sealer - where hot air is blown toward both edges of the blank. The purpose is to melt the polymer layer at the heated edges. Later the edges are folded onto each other, resulting in a sealed sleeve.

The process in the side sealer can lead to overheat on machine parts, malfunction and therefore decrease of the throughput of the complete production line. In this thesis numerical simulations were used to identify the critical thermal deformations of the side sealer parts and understand the root cause. Thereafter multiple concepts were generated and the simulations results showed their impacts on the side sealer performance.

In this work, we used a product development methodology, in which numerical simulations are used to develop and validate potential concepts. In total, three concepts were implemented, simulated and analyzed. The first concept is to make small cuts in certain regions, where large magnitudes of thermal deformation were observed. The second concept delved into a potential material change, to use aluminum instead of the typical stainless steel. The last concept is a classic engineering solution, adding beams to reinforce the identified problematic areas.

Keywords: Computational fluid dynamics, Finite element method, Simulations, Product development, Side sealer.

Sammanfattning

I detta examensarbete, numeriska simuleringsverktyg - CFD och FEM - användes för att beräkna flödet, temperaturfältet och de termiska deformationerna inuti en maskin för försegling av den vertikala kanten av en kartongförpackning. Arket - förpackningsmaterialet har en U-form - matas in i maskinen - side sealer - där varm luft blåses mot båda kanterna av arket. Syftet är att smälta polymer lagret på kanterna. Därefter viks kanterna mot varandra, detta resulterar till en kapsel.

Denna processen i side sealer kan leda till överhettning av maskin komponenter och därmed minska den totala produktionen. I detta examensarbetet har numeriska simuleringar använts för att identifiera de kritiska termiska deformationer av side sealer komponenter och förstå grundorsaken. Därefter utvecklades flera koncept och simulerings resultaten visade deras påverkan på maskinens prestation.

I detta arbete, använde vi en produktutvecklingsmetod, där numeriska simuleringar används för att utveckla och validera koncept. Totalt, tre stycken koncept implementerades, simulerades och analyserades. Det första konceptet är att införa små genomskärningar i vissa regioner, där de högsta termiska deformationer observerades. Det andra konceptet undersökte ett potentiellt materialbyte, att använda aluminium istället för den typiska rostfritt stål. Det sista konceptet är en klassisk ingenjörslösning, att tillägga balkar för att förstärka identifierade problematiska områden.

Nyckelord: CFD, FEM, Simulering, Producktutvecklingsmetod, Side sealer.

Acknowledgments

I would like to express my sincerest gratitude to Dr. Aurelia Vallier at Tetra Pak for giving me the opportunity to conduct my master's thesis at Tetra Pak and for her guidance and support throughout this thesis. Many thanks to Johan Nordgren at Tetra Pak for his support and feedback.

Words cannot express my gratitude to my supervisor Axel Nordin at Lund university for his support and guidance. I would also like to thank my co-supervisor Lars Palm for his help.

Moreover, I am very grateful to the employees at Tetra Pak who welcomed and supported me throughout this project.

Lastly, I would like to thank my family for their endless love and support, this journey would not have been possible without them.

Lund, May 2026

Mikael Karlsson

Table of Content

1 Introduction

This section introduces Tetra Pak, the description of the problem, the purpose of the thesis, the delimitations, and the structure of the thesis.

1.1 Background

Tetra Pak is a Swedish company that provides advanced food production systems. The company was founded in 1951 by Dr. Ruben Rausing in Lund. Initially, Tetra Pak introduced the classical tetrahedron-shaped package for milk. A year after the company was founded, the first filling machine was delivered to the Lund dairy with the purpose of filling the classic tetrahedron-shaped package. Afterwards, Tetra Pak expanded its business portfolio through the continuous development of packaging solutions and food processing [1].

For some packages produced in Tetra Pak machine, the sealing of the longitudinal seam is performed in a side sealer machine. In this machine, hot air jets heat the edges of the packaging material, melt the polymer layer and act as a glue when the package material is folded. Due to the continuous production of these packages, some of the side sealer machine parts are subjected to a large amount of heat, which can lead to overheating of specific machine components. In this thesis, the flow, heat distribution and thermal deformations in a side sealer machine is studied.

1.2 Problem Description

It is not well understood why specific parts of the side sealer overheat during production. This overheating leads to machine jamming, and decrease of the throughput. In order to understand the root cause, we want to utilize simulation tools with the intention of visualizing the problems that are occurring during production. The same simulations can thereafter be used to validate concepts, to minimize overheating. This approach will enable a higher throughput of the production line and thereby reduced total costs.

In this thesis, the air flow, the heat and the thermal deformation in the side sealer machine will be studied extensively. This will be done by setting up multiple CFD (computational fluid dynamics) and FEM (finite element method) simulations. This will help identify the main problems that occur during production and the simulations will be used to validate multiple concepts that will be generated through the project.

1.3 Purpose and Objectives

The purpose of this thesis is to simulate sealing of the blanks (packaging material) process, analyze which specific parts of the side sealer machine overheat, and then propose solutions to minimize the thermal deformations. During the project, it was discovered that the critical thermal deformation is present in the outer plate see Figure 4.1. Namely that the resulting thermal deformation is greater than 2 mm in the Z-axis, Figure 5.18. This is a problem since the distance from the outer plate to the blanks (red parts in Figure 4.1) is less than 2 mm. The purpose is fulfilled through the completion of the following objectives:

- CAD-cleaning of the existing assembly of the side sealer machine.
- Extract the fluid region that is enclosed within the assembly.
- Complete CFD-simulation of the flow and heat transfer within the side sealer.
- Complete FEM-analysis of the thermal deformations of specific machine parts.
- Define a potential design change, adapt the geometry and settings, rerun the simulations, analyze and compare the results to the reference geometry, Figure 5.18.
- Share the analyze and comparisons with stakeholders.

1.4 Delimitations

The scope of this thesis includes capturing the current failure mode of the side sealer machine through numerical simulations and utilizing the models to validate potential solutions. Multiple design simplifications were made to allow the simulations to run without problems and to minimize the simulation time. All parts that are in contact were combined into one geometry, rather than having separate geometries, this results in very high stresses in certain regions. However this is not a problem given the scope of the thesis, since the thermal deformations were the main interest and are not affected by the resulting stresses.

The exact details regarding the implementation of the solutions will be excluded in this thesis. Furthermore, no cost calculations will be performed for each solution, and the electrical components of the production machine are not considered throughout the thesis work. The main reason for this is to be able to generate concepts more freely.

1.5 Structure of the Thesis

The structure of this thesis follows the LTH's guidelines for scientific reports. The thesis starts with an introduction, followed by an explanation of the theory and method used. Afterwards, the simulation setup and results are described. Lastly, the remaining future work and conclusions are presented.

2 Theory

This section will describe the relevant theory utilized in this thesis. The basic theory of CFD (computational fluid dynamics) and FEM (finite element method) is presented, along with the necessary steps to run a CFD and FEM simulations

2.1 CFD Theory

The conservation of mass equation, see Equation 2.1, the conservation of momentum equation, see Equation 2.2, along with the conservation of energy equation, see Equation 2.3 are the equations that computational fluid dynamics (CFD) mainly solves. In table 2.1, the corresponding nomenclature for Equations 2.1-2.3 can be seen.

$$\frac{dp}{dt} + \nabla \times (\rho \vec{V}) = 0 \tag{2.1}$$

$$\rho \frac{d\vec{V}}{dt} + \rho(\vec{V} \times \nabla)\vec{V} = -\nabla p + \rho \vec{g} + \nabla \times \tau_{ij} \tag{2.2}$$

$$\frac{d(\rho E)}{dt} + \nabla \times (\vec{V}(\rho E + p)) = \nabla \times (k \nabla T) + S_h \tag{2.3}$$

Table 2.1: CFD nomenclature.

Variable	Property	Unit
p	Pressure	Pa
V	Velocity	m/s
ρ	Density	kg/m^3
g	Acceleration	m/s^2
τ	Shear stress	Pa
E	Specific internal energy	J/kg
T	Temperature	K
k	Thermal conductivity	W/mK
S	Other energy sources	W/m^3

The equations are non-linear partial differential equations (PDE), making them often not possible to solve analytically for most real world problems. With a CFD method, these equations are rather solved numerically, resulting in an approximate solution. This is done through defining a discrete domain instead of a continuous one and solving for those specific discrete regions and then interpolating the results, resulting in an approximate solution to the continuous problem. For the interested reader, read the following References [2], [3] and [4] for a more in-depth explanation of the CFD method.

2.2 CFD Simulation Basics

The CFD simulations that were carried out in this thesis used the software Simcenter STAR-CCM+. The basic requirements for a CFD simulation can be seen in Figure 2.1.

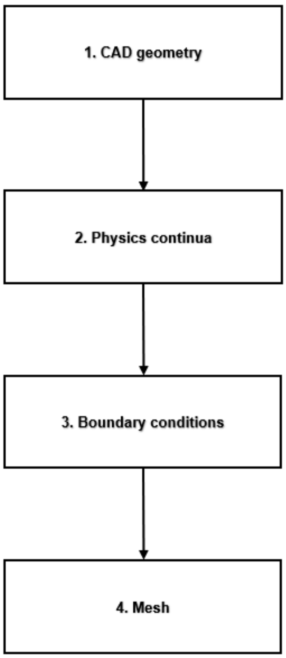

Figure 2.1: Basic steps to perform in order to run a CFD simulation.

At the start of any CFD simulation, a CAD geometry is required, this can be parts that are either imported into the simulation or created within the simulation software. This includes the fluid regions as well. The CAD geometry used is described in Section 4.1. Once the CAD geometry is defined within the software, the next step is to set up the physics continua of each region. A physics continua contains the material properties of a material, such as type of material, the density properties, gas/fluid properties, etc. The solver also has to be defined under physics continua. A solver is the set of equations that will be used to solve the CFD problem, this includes whether the problem is steady or transient, the solving approach such as segregated or coupled flow, etc. For the defined physics continua and the reasoning as to why they are chosen, see Section 4.2. Afterwards, boundary conditions have to be defined on each part surface, such as inlet, outlet, walls, etc. One has to define the boundary conditions before generating the mesh, since the meshing technique utilized will depend on the defined boundary conditions. A mesh is a way of making the region into a discrete domain, as mentioned before in Section 2.1. Star-CCM+ will use this discrete domain and solve the governing equations over each cell using the finite volume method [5]. There are three different core volume meshes called polyhedral mesh, tetrahedral mesh, and trimmed cell mesh. Moreover there are different meshing strategies. In areas in which highly dynamic flows are expected, having a finer mesh is preferred to not miss any important details and it is also required in the area where heat transfer occurs. While in other regions a coarser mesh can be used to save computational resources. A Mesh study in the crucial regions has to be carried out in order to ensure that the generated mesh is adequate. This is done by halving the mesh size and observe the change in results. If the change in the final results is marginal (about 5 to 10 percent difference), then it is safe to assume that the mesh is sufficient, if this is not the case then one needs to continue this process. In Section 4.3, the boundary conditions and mesh settings, and the reasoning behind each chosen setting can be seen. Post-processing is the last step of any CFD simulation, this step includes setting up plots, creating visualization scenes, etc. to analyze the results.

2.3 FEM Theory

A similar approach to CFD is used in FEM, where non-linear partial differential equations that are solved numerically. One of the most fundamental equations in FEM is called the Poissons equation, see the equation below,

$$-\vec{\nabla} \times (k\vec{\nabla}u) = f \tag{2.4}$$

One of the reasons as to why it is a fundamental equation lies in its versatility, it can be used to solve problems in different branches of physics. Two popular examples are within the heat diffusion and elasticity related problems. For the heat diffusion problem, u is the temperature field, k is the heat conductivity, and f would be the heat source. This is often denoted as the following,

$$u = T \tag{2.5}$$

$$f = \vec{q} \tag{2.6}$$

In the case of elasticity, u is the displacement vector, k is the tensor of elastic constants, and lastly, f is the force density. This is often defined as the following,

$$u = \vec{u} \tag{2.7}$$

$$k = \overline{\overline{C}} \tag{2.8}$$

$$f = \vec{f} \tag{2.9}$$

For further reading on FEM theory, see [6], [7] and [8]. In this thesis, the temperature will be solved using CFD and then used as an input for the FEM solver to calculate the thermal deformation [9], see Equation 2.10. In Figure 2.2, the nomenclature for the FEM theory can be seen.

$$\epsilon = \alpha \Delta T \tag{2.10}$$

Table 2.2: FEM nomenclature.

Variable	Property	Unit
T	Temperature	K
$\vec{q}$	Heat source	W/m^2
$\vec{u}$	Displacement	m
$\overline{\overline{C}}$	Elastic constant	N/m^2
$\vec{f}$	Force density	N/m^3
ϵ	Thermal strain	-
α	Coefficient of thermal expansion	1/K

2.4 FEM Simulation Basics

FEM simulations were performed, using the software HyperMesh, with the Abaqus solver. Similarly to CFD simulations, there are basic steps that needs to be defined before one can perform the simulation, see Figure 2.2.

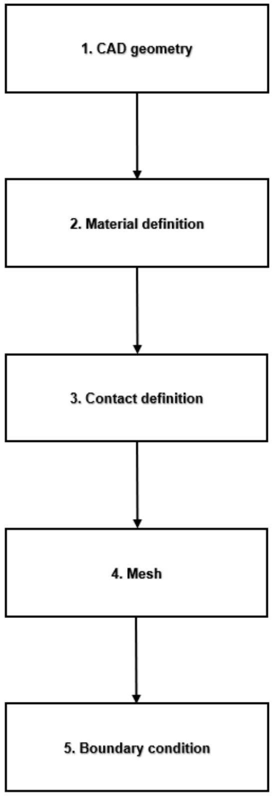

Figure 2.2: Basic steps to perform in order to run a FEM simulation.

The first step is to create or import the CAD geometry into the FEM software. The CAD geometry can be either imported from other CAD software, or created directly in HyperMesh. Afterwards the material is defined for each CAD component. In the common case of a simulation on an assembly of parts, contact definition between the different parts needs to be set, there are both linear and non-linear definitions. The contacts can be bonded, frictionless, frictional, etc. Thereafter, a mesh has to be created, there are multiple types of mesh elements that can utilized, for example hexahedral, tetrahedral, etc. The choice of mesh depends on multiple factors, one example is the complexity of the geometry, for example hexahedral mesh can be used for simpler geometries and the tetrahedral mesh can be used for complex geometries [10]. Afterwards one needs to specify the boundary conditions, this includes the forces and temperature on specific parts, supports such as fixed support, etc. The settings utilized in this project for the FEM setup is described in Section 4.8. The last step is post-processing, which consists of visualizing the resulting stress, resulting deformation, create plots and more.

3 Method

This section presents the methodology used in the thesis. Each step of the predictive design analysis is described.

3.1 Predictive Design Analysis

The main driver for this thesis is the continuous use of numerical simulations to vizualise the flow, heat and deformations in the side sealer machine. The simulation results will help to understand the current problem that occurs during production. Once the simulation model has been set-up and its results validated, it can be reused when design changes are made. The development of a solution for the problem described in this thesis will largely be influenced by the simulation results, therefore, a methodology for predictive design analysis (PDA) will be utilized [11]. The high-level steps for the PDA methodology are three consecutive steps, see Figure 3.1.

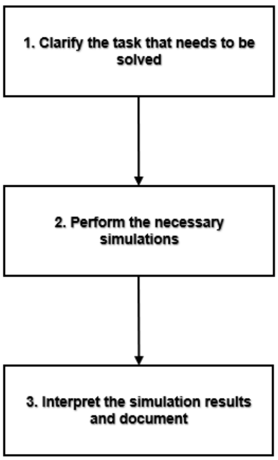

Figure 3.1: High-level steps for PDA methodology.

Within each step there also exist three additional sub steps that each form the high-level steps, the steps can be seen in Figure 3.2. At the start of any given project, one has to identify the task, in the case of this thesis it is to minimize the thermal deformation. Once the task has been identified, a goal needs to be defined, meaning at which point the task is considered solved. Afterwards one needs to plan and communicate the said plan to everyone involved in the project. In the second step, simulations are performed, this includes pre-processing, running the simulation and then post-processing. The last step is directly tied to post-processing, once the results are extracted, it is important to both understand and assess whether the results are reasonable. If the results are deemed to be acceptable, all that remains is to document the findings and then integrate them into the project, for further reading, see Reference [11].

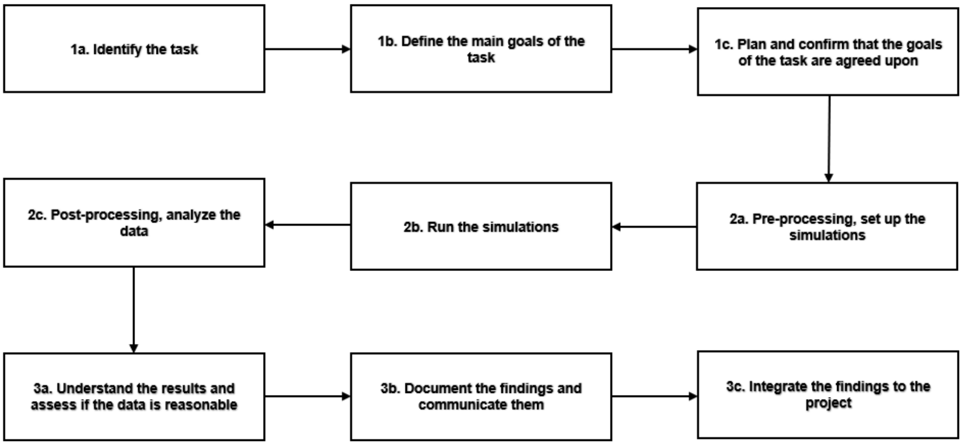

Figure 3.2: Sub steps within each high level step.

4 Simulations

In this section, both the CFD and FEM simulation setups are presented in great detail.

4.1 Background for the Simulations

The main principle of the side sealer machine that is studied in this thesis is that hot air is flowing out of nozzles onto the packaging material (PM) and this melts the polymer layer on designated areas of the PM. In total, there are five nozzles, three on the driver side (DS) and two on the operator side (OS). Multiple vacuum boxes are present in the machine and their purpose is to ensure that the PM stays in the desired position by applying outward pressure on the vertical walls of the blanks. The blanks are constantly moving through the machine, this motion is not resolved but modeled in the simulation by setting wall velocity as a boundary condition on the PM parts. Lastly, the purpose of the thesis is to minimize machine parts overheating, which often results in forced stoppage of production. The culprit of this overheating is a certain outer plate that exists in close proximity to the nozzles. The discussed CAD geometry can be seen in Figure 4.1.

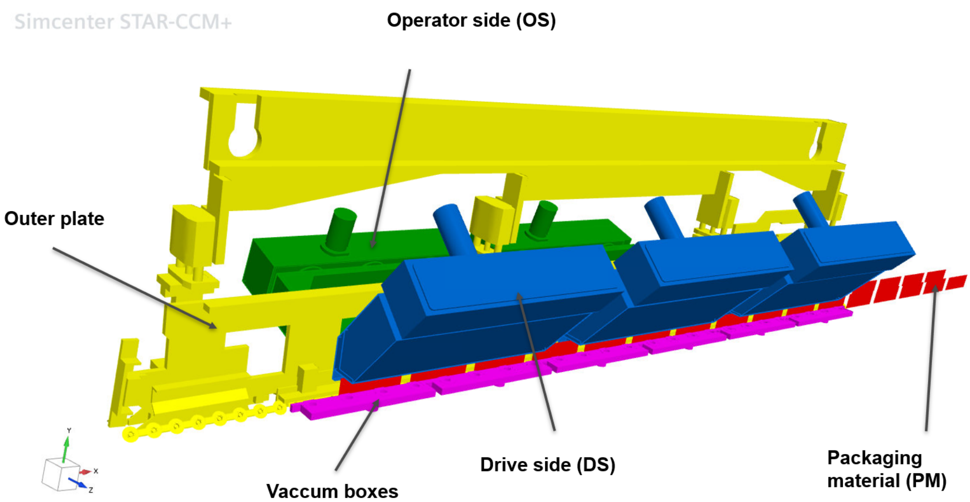

Figure 4.1: The CAD geometry in Star-CCM+.

In Figure 4.2 DS nozzles are shown, and the air pathway within the inner part of the DS nozzles can be seen in Figure 4.3. The nozzle outlets consist of multiple small pipes, see Figure 4.4. When the air flow exists the nozzles through these pipes, it leads to multiple hot air jets toward the blanks.

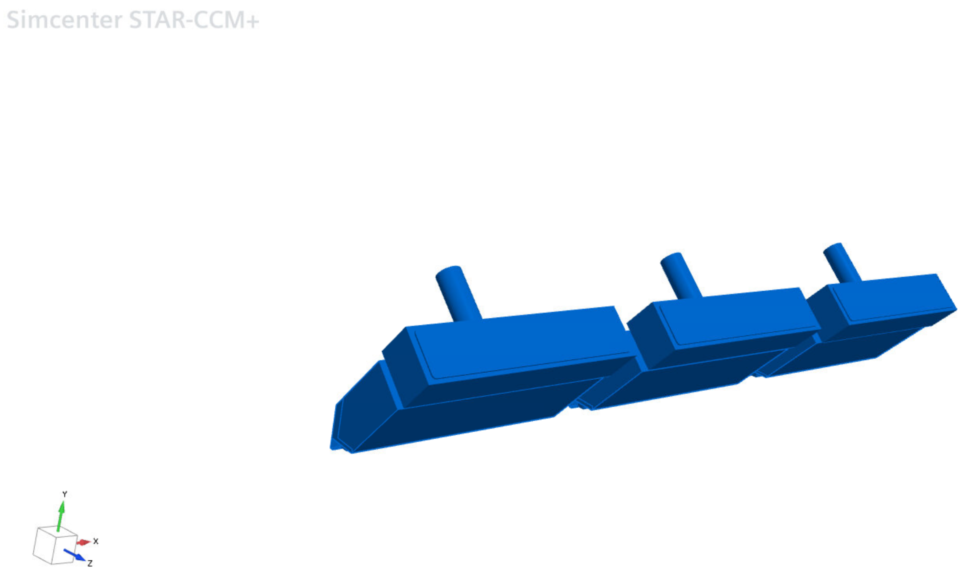

Figure 4.2: The geoemtry of the DS nozzles.

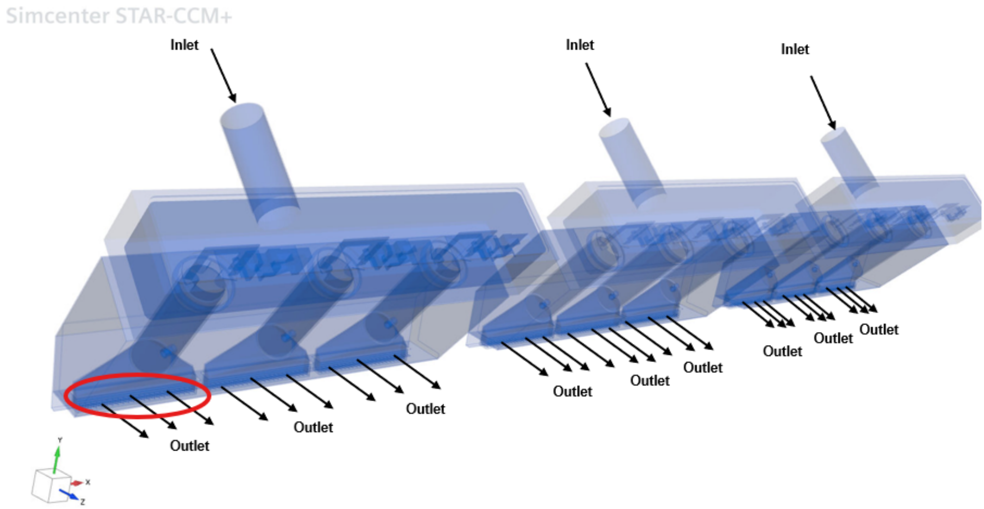

Figure 4.3: Inner parts of the DS nozzles and air pathway.

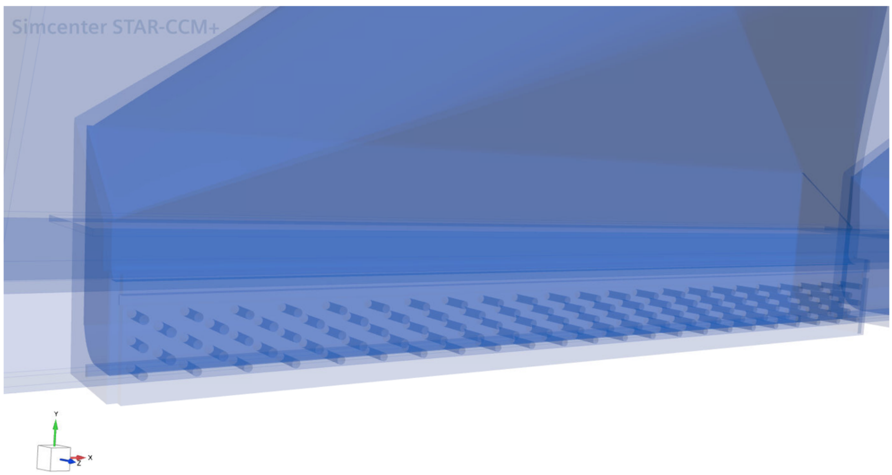

Figure 4.4: Zoomed in near the nozzle outlets, at the location marked in red in Figure 4.3.

4.2 Physics Continua Definition

A model of the flow and heat transfer on the DS side of the side sealer has already been implemented at the virtual modeling group at Tetra Pak. This model consists of two simulations, one evaluates the flow in a single nozzle, then the flow properties are extracted at the nozzle outlets, mapped on the others nozzles and thereby used as boundary conditions in a second simulation where the flow is calculated in the whole side sealer. This approach and the simulation set-up was thoroughly studied in the beginning phase of the thesis and was used as a guideline for performing the CFD simulations presented in this report. The physics continua for five different materials -air, aluminum, board, polypropylene (PP) and steel- are defined in Star-CCM+. Table 4.1 and 4.2 show the physics continua defined for the air flow and solid materials respectively.

Table 4.1: Physics continua for air.

Cell Quality Remediation
Gas
Gradients
Ideal Gas
K-Epsilon Turbulence
Realizable K-Epsilon Two-Layer
Reynolds-Averaged Navier-Stokes
Segregated Flow
Segregated Flow Temperature
Solution Interpolation
Steady
Turbulent
Two-Layer All y+ Wall Treatment
Wall Distance

Table 4.2: Physics continua for the solid materials.

Constant Density
Gradients
Segregated Solid Energy
Solid
Solution Interpolation
Steady
Three Dimensional

For the fluid modeling, the ideal gas model is suitable in this case to describe the physics for air. The goal of the simulation is to obtain an overall picture of the flow and since the flow is relatively simple, the segregated flow, steady, solution interpolation options are chosen. The cell quality remediation and gradients options are chosen to increase the robustness of the solutions. These models will identify the poor quality meshes and ensure that the computed data in these meshes are not deviating from the overall solved data, which will aid in convergence. The segregated flow temperature model is picked to solve the energy equation. The flow is expected to be turbulent, therefore the Realizable K-Epsilon Two-Layer option is selected to model the turbulence. The K-Epsilon turbulence and Reynolds-Averaged Navier-Stokes (RANS) are the chosen turbulence models. There exist a wide variety of turbulence models, each having their respective strengths and weaknesses, the ones utilized in this case are often used in industrial settings [12]. The reason why they are often used in industry is their effective use of computational resources, while ensuring an accurate solution for the overall flow and heat transfer. Therefore, the chosen turbulence model is ideal, since the turbulence will be accurately solved, while allowing for relatively fast simulations, when compared to other models. The treatment of the turbulence near the wall is controlled by, the last two settings.

In the table for the solid materials, see Table 4.2, the density is assumed to be constant, this will result in a simpler model, but is sufficient for this project. There are two other density models in Star-CCM+, namely the polynomial density and the user defined EOS. The polynomial density will change the density of the material depending on the temperature. For the user defined EOS density model, one can define the properties to a very high extent, for example the density can depend on the temperature, pressure, etc. In the case of solid materials, the segregated solid energy setting is recommended for heat transfer related simulations. The remaining options are there to increase the robustness of the simulation, similar to the ones chosen in Table 4.1.

4.3 One Nozzle DS CFD Simulation

4.3.1 One Nozzle DS Simulation Geometry

In order to save computational time, one nozzle of each side is simulated and the computed flow properties at the nozzle outlets will be extracted and mapped on the outlets of all five nozzles. The overall computational domain for the one nozzle DS simulation can be seen in Figure 4.5, the geometries surrounding the nozzles were simplified, since the main purpose of this simulation is to obtain the flow properties at the nozzle outlets shown in Figure 4.4. The results in fluid domain will be visualized on the 2D plane in Figure 4.6. The inner part of the DS nozzle consists of three fluid regions, see Figure 4.7, where the region 2 corresponds to a heater which is described as a porous region to obtain the appropriate pressure distribution across this region.

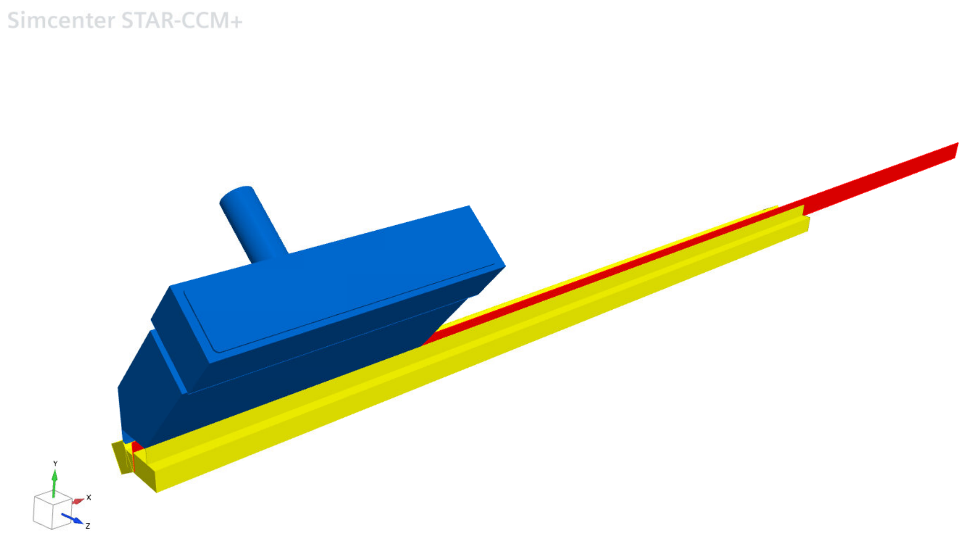

Figure 4.5: CAD geometry used for the one nozzle simulation, same positioning as the one in Figure 4.1.

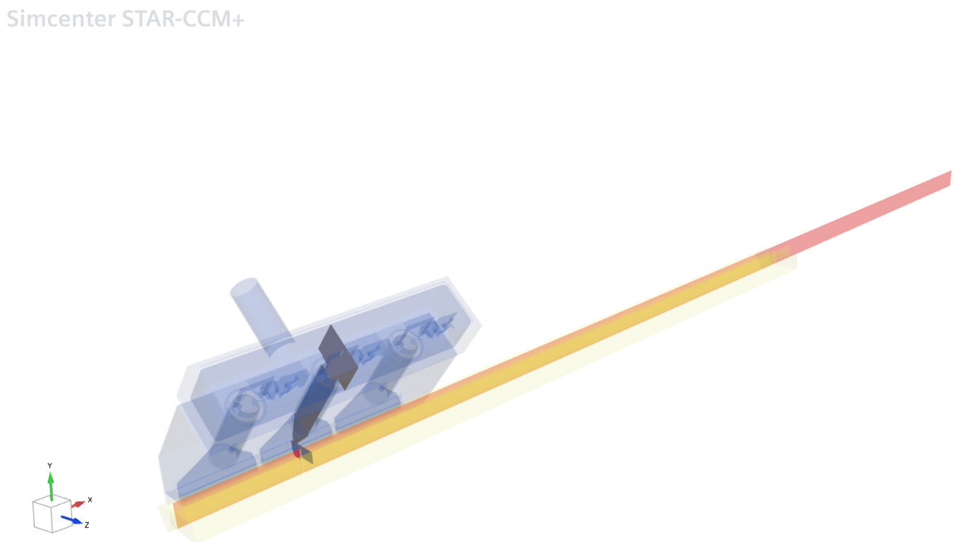

Figure 4.6: The position of the 2D plane.

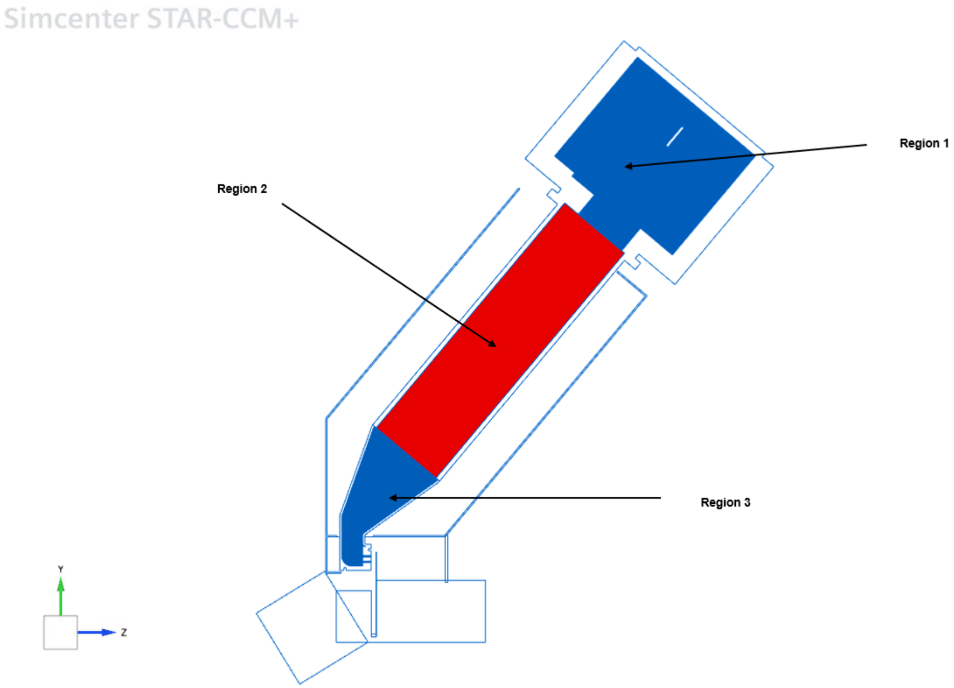

Figure 4.7: The three fluid regions within each nozzle.

4.3.2 Region Definition and Set Up

The boundary conditions in the fluid region are shown in Figure 4.8, they are wall boundaries (blue), mass flow inlet at the fluid inlet surface in region 1 (green), and interfaces (yellow) defined at the contact areas between the 3 regions within the nozzle and between region 3 and the surrounding air at the nozzle outlets.

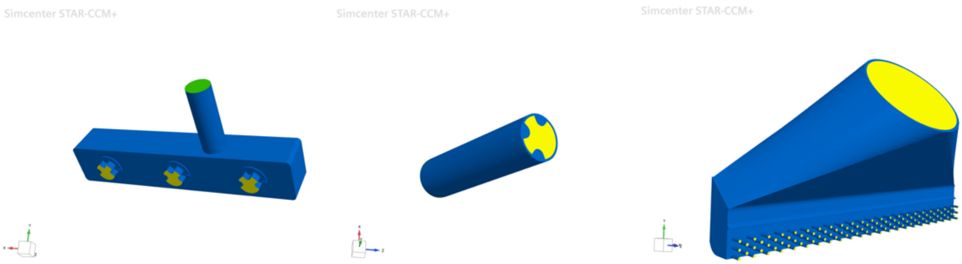

Figure 4.8: Boundary conditions and interfaces for the fluid domain regions

The region type for region 2 is porous, which is a regular fluid region, with the addition of resistance, meaning that in this region the fluid flows freely but is slowed down. This is used to model the slower airflow through the heaters.

The last regions define the packaging material. The properties of the packaging material and its structure is classified and will not be disclosed in this thesis. It consists of multiple layers with different materials that are connected and each layer has its own physics continua, see Table 4.2. In addition, interfaces are defined on surfaces in which the layers are connected. The blanks' motion is modeled with a wall velocity boundary condition, and the "convective velocity" option is chosen to account for the motion in the energy equation.

4.3.3 Mesh Generation

The basic mesh settings used for the CFD simulation can be seen in Table 4.3. The prism layer mesher is used exclusively in fluid regions, since the purpose of this setting is to capture effects of turbulence near solid walls [13].

Table 4.3: Basic mesh settings for the fluid regions.

Surface Remesher
Automatic Surface Repair
Trimmed Cell Mesher
Prism Layer Mesher

The trimmed cell mesher is utilized due to its effective use of computational resources [14] when studying conjugate heat transfer (CHT). The surface remesher and automatic surface repair are selected to automatically improve the mesh through multiple iterations. For more detailed information regarding mesh size, number of prism layers, etc. see Tables 4.4-4.6.

Table 4.4: Mesh settings for the surrounding air region.

Property	Value
Base Size [mm]	2
Number of Prism Layers [-]	5
Prism Layer Reduction Percentage [-]	25
Near Core Layer Aspect Ratio [-]	0.6
Gap Fill Percentage [-]	49
Minimum Thickness Percentage [-]	0.1
Prism Layer Total Thickness, Percentage of Base [-]	80
Volume Growth Rate, Default Growth Rate [-]	Slow
Volume Growth Rate, Surface Growth Rate [-]	Slow
Maximum Cell size, Percantage of Base [-]	100

Table 4.5: Mesh settings for the fluid regions within the nozzle.

Property	Value
Base Size [mm]	2
Number of Prism Layers [-]	5
Prism Layer Total Thickness, Percentage of Base [-]	80
Surface Growth Rate [-]	Slow
Volume Growth Rate, Default Growth Rate [-]	Slow
Volume Growth Rate, Surface Growth Rate [-]	Slow
Maximum Cell size, Percantage of Base [-]	100

Table 4.6: Mesh settings for the solid region.

Property	Value
Base Size [mm]	10
Number of Prism Layers [-]	5
Prism Layer Total Thickness, Percentage of Base [-]	2

Near core layer aspect ratio, gap fill percentage and minimum thickness percentage are settings for the prism layers. When applying their default values in the surrounding air region, problems arose when attempting to generate the mesh, often in the form of negative volume cells being created. This indicates that the mesh is too coarse in certain regions. Therefore, the values were refined until the problems disappeared. The growth rate settings are set to slow or very slow, ensuring that there are no large differences in size between neighboring meshes. In the region 3, the growth settings were changed to very slow. The allowed maximum cell size is set to be as large as the defined base size. Prism layer thickness is different for some regions, as one can see in the Tables 4.4-4.6, in the regions where the flow velocities and temperature variations are expected to be low, a larger prism layer thickness is applied. In the fluid nozzles, the pipes of the nozzle outlets have a small diameter, and the prism layer thickness is lowered to predict an accurate flow velocity field of the hot air jets.

A mesh study was performed, in order to validate the choice of the mesh settings. The temperature on a probe line (shown in purple in the Figure 4.9) was compared for the base size (4, 2 and 1 mm) and the number of prism layers (2,5 and 10). In Figure 4.10, the temperature plot for the different mesh settings can be seen. With a coarser mesh, the temperature is under-predicted with 19 degrees, while the finer mesh gives similar results as the medium mesh while the computational time is increased with 10000 seconds. With the lowest number of prism layers, the temperature is under-predicted and the higher value does not improve the accuracy compare to having 5 prism layers, see Figure 4.11. In Table 4.7 the maximum air velocity, and the computational time are compared for the different meshes, and a good compromise between accuracy of the results and computational time is obtained with a base size of 2 mm and 5 prism layers on the walls exposed to high temperatures.

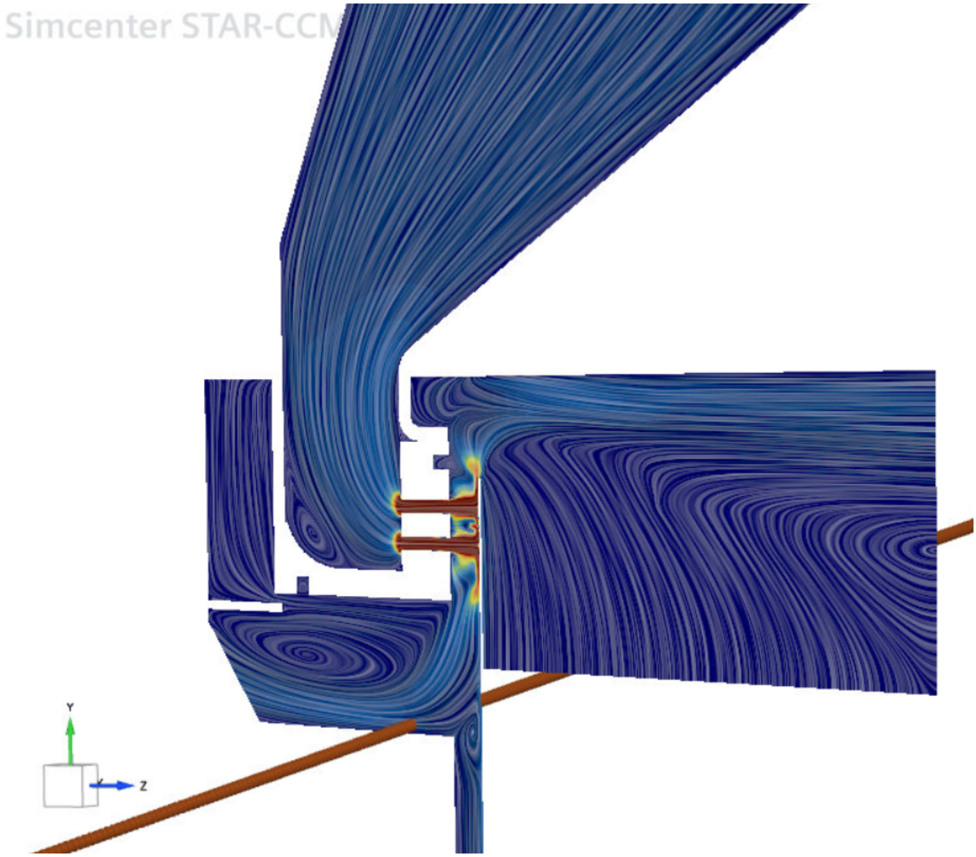

Figure 4.9: Line probe.

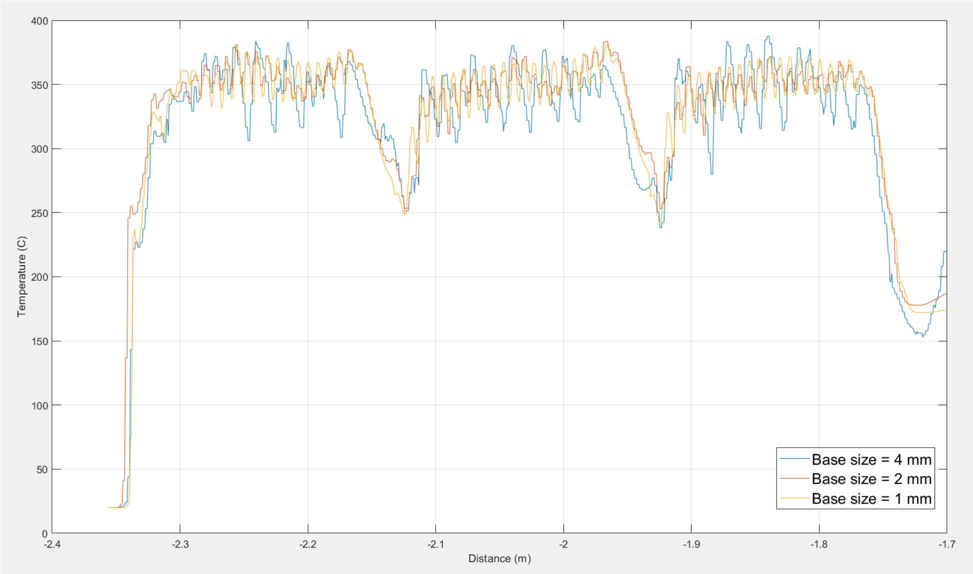

Figure 4.10: Resulting temperature for each base size of the mesh on the probe line (MATLAB was used to generate this plot).

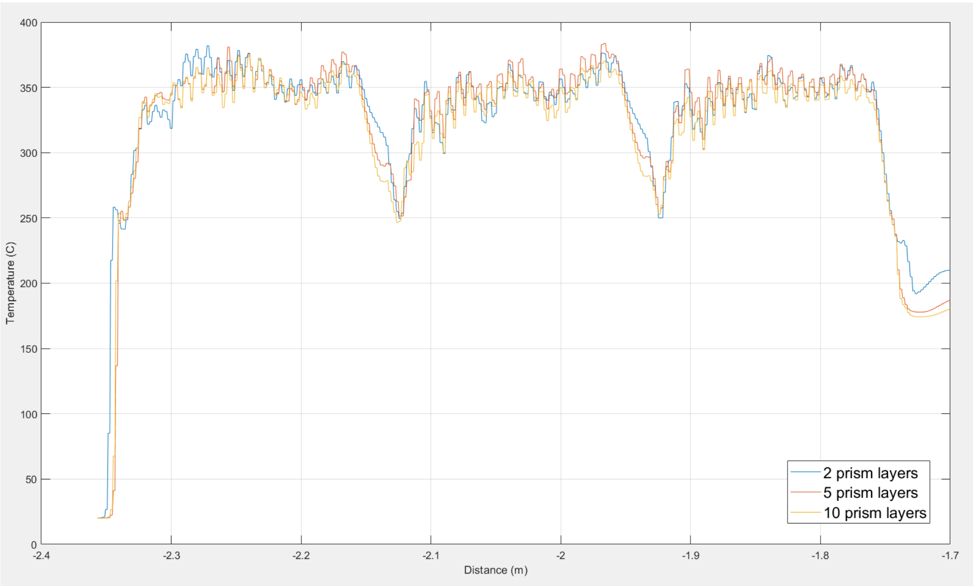

Figure 4.11: Resulting temperature for different amounts of prism layers on the probe line for the base size 2 mm (MATLAB was used to generate this plot).

Table 4.7: **Mesh base size, maximum air velocity, time for the simulation to run and iterations.**

Base size [mm]	Maximum air velocity [m/s]	Time to compute [s]	Iterations [-]
4	100	480	700
2	85	1370	700
1	84	6130	700

To obtain an accurate prediction of the flow and heat transfer out of the nozzles, refinement blocks were created in the region of the hot air jets, see the Figures 4.12 and 4.13 (pink blocks). The settings applied to the mesh refinement region can be seen in Table 4.8. The size for the refinement region is 5 percent of the base size, with an uniform relative size for each axis. The prism layer thickness is 8.5 percent of the base size on the blanks wall, ensuring that the heat transfer between the hot air jets and the packaging material walls is properly captured.

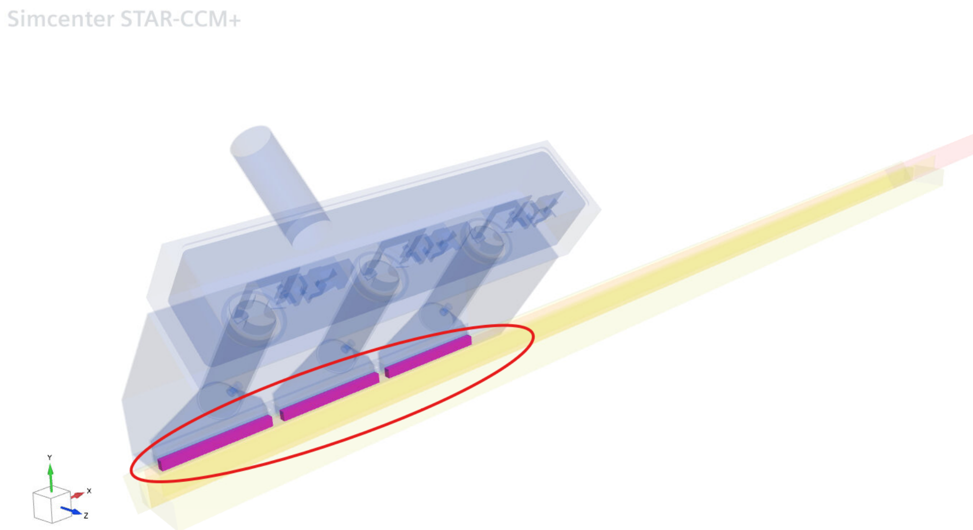

Figure 4.12: Mesh refinement regions.

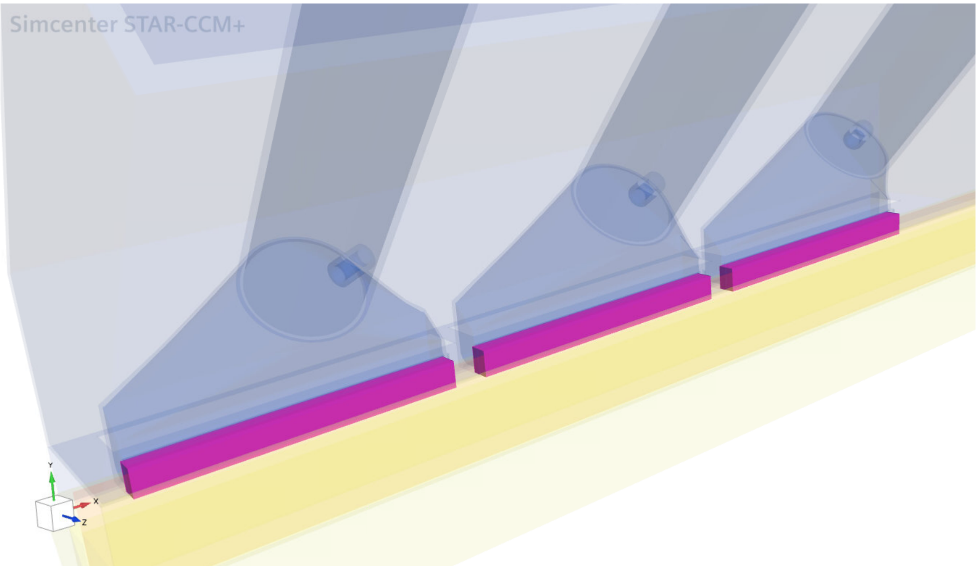

Figure 4.13: Mesh refinement regions zoomed in at the circle seen in Figure 4.12.

Table 4.8: Volumetric control setting for the refinement regions.

Property	Enabled/Value
Surface Remesher	Enabled
Prism Layer Mesher	Customize Number of Layers and Customize Total Thicknes enabled
Trimmer	Customize Anisotropic Size enabled
Custom Size, Relative to base [-]	5
Relative X Size, Percentage of Base [-]	10
Relative Y Size, Percentage of Base [-]	10
Relative Z Size, Percentage of Base [-]	10
Prism Layer Total Thickness, Relative to base [-]	8.5

Furthermore the prism layer mesher are disabled at the interfaces. This was done by defining a new custom surface control. The final generated mesh for the one nozzle DS case can be seen in the Figure 4.14 and the zoomed in region in Figure 4.15 where the finer at the refinement region is highlighted, along with the disabled prism layer at the interfaces.

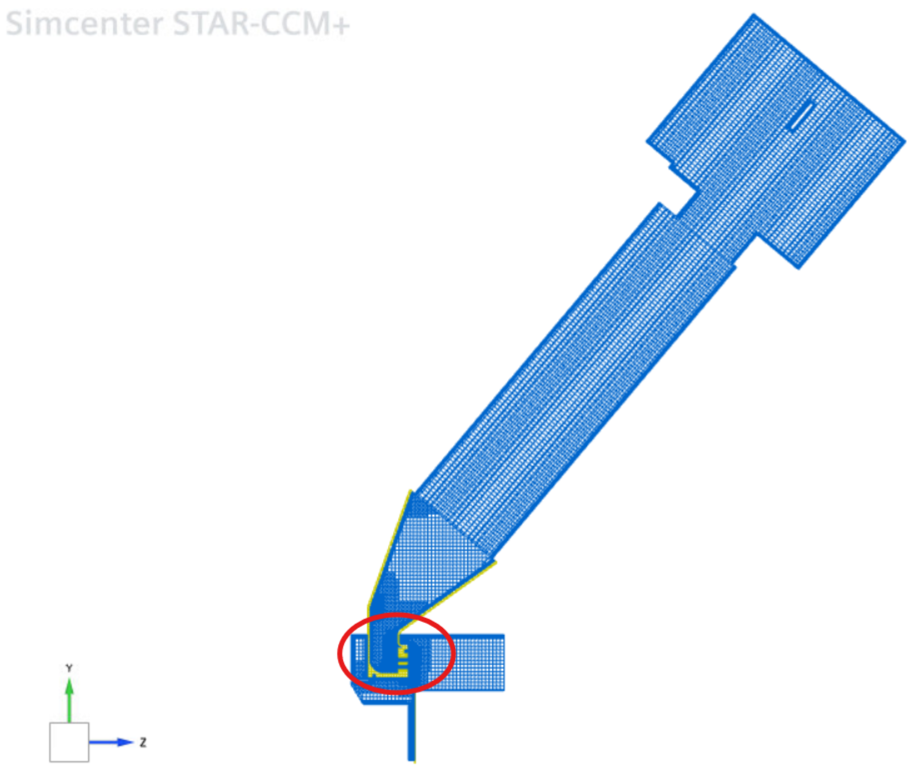

Figure 4.14: The mesh at the 2D plane that can be seen in the Figures 4.6 and 4.7.

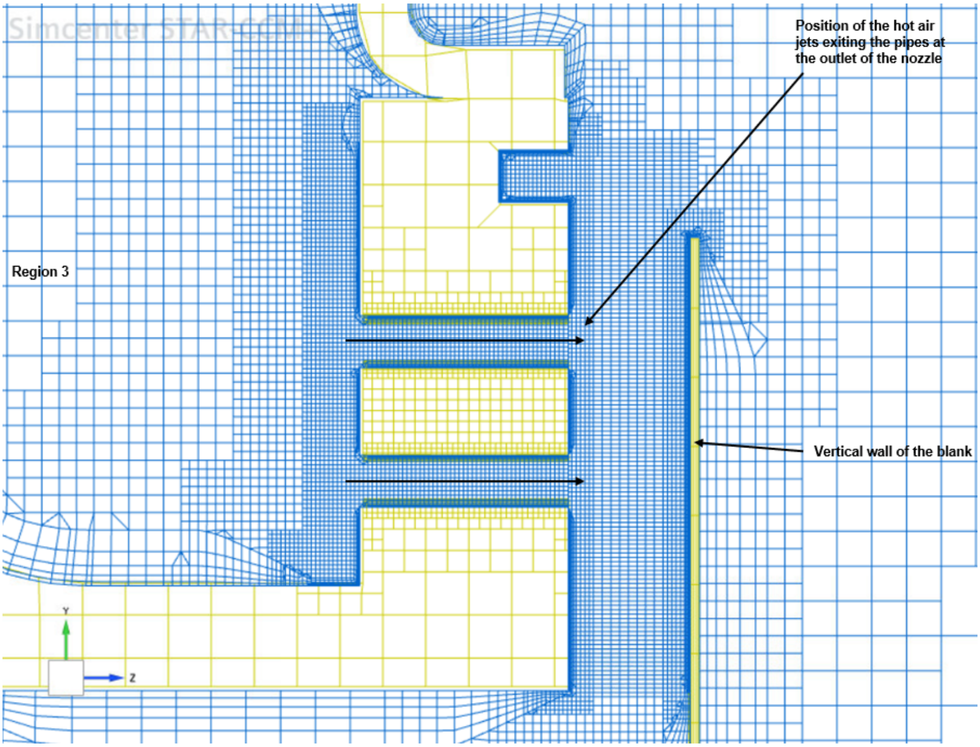

Figure 4.15: Zoomed in image at the circled out location in Figure 4.14. The mesh of the fluid regions in blue, and the solid regions in yellow.

4.4 One Nozzle OS CFD Simulation

4.4.1 One Nozzle OS Simulation Geometry

The CAD geometry for the one nozzle OS simulation can be seen in Figure 4.16 and the nozzle geometry is the same as shown in Figures 4.3 and 4.4. The fluid domain seen in Figure 4.7 was used for the simulations of the OS side as well.

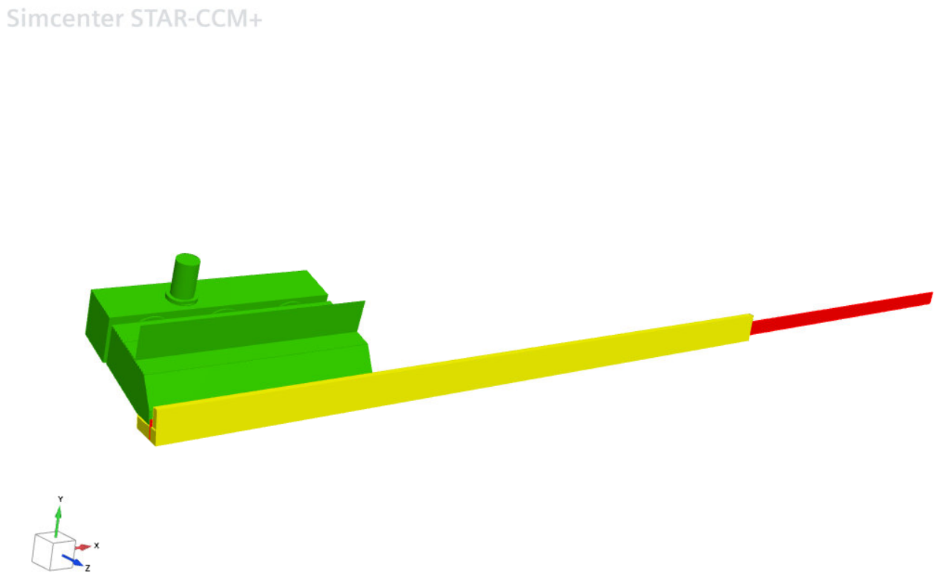

Figure 4.16: The one nozzle OS geometry.

4.4.2 Region Definition and Set Up

The same boundary conditions and interfaces that were observed in Section 4.3 were used. In addition, the same mesh settings were utilized, including the mesh refinement regions in front of the nozzle outlets and the disabling of the prism layers at interfaces. The same geometry regarding the mesh refinement regions were used, only exception being that it had to be moved along the Z-axis so that it accounts for the OS side instead. A 2D plane, such as the one seen in Figure 4.6, is where the resulting mesh will be visualized. The mesh can be seen in the Figures 4.17 and 4.18.

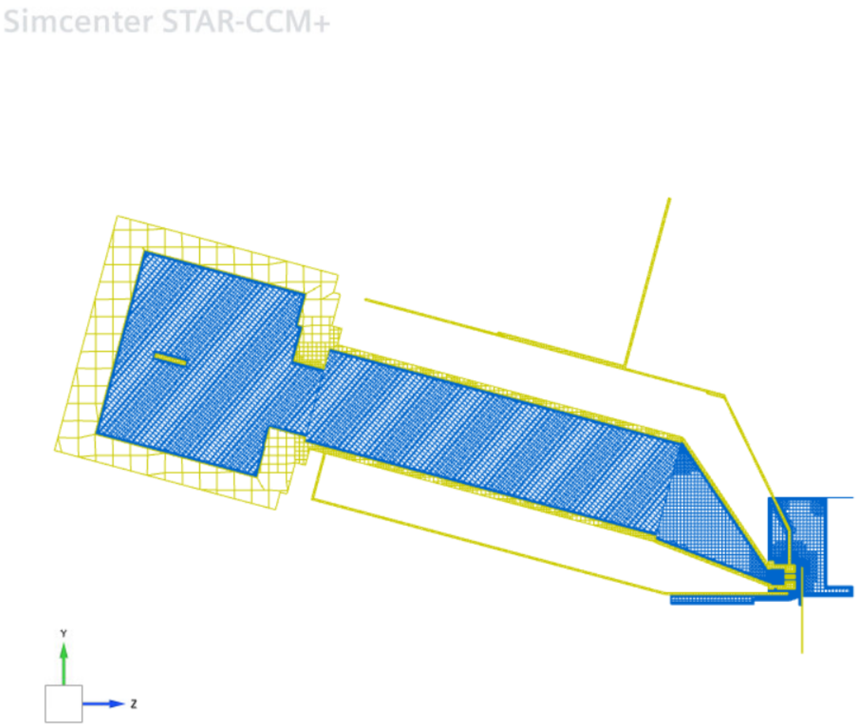

Figure 4.17: The mesh for the one nozzle OS simulation.

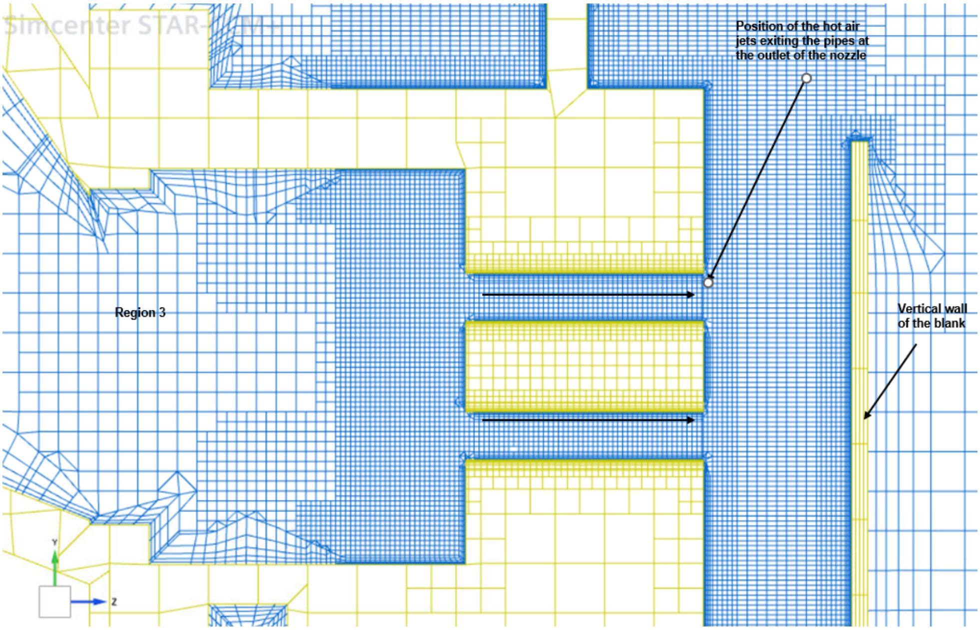

Figure 4.18: Zoomed in figure at the nozzle outlet mesh for the one nozzle OS simulation.

4.5 Three Nozzle DS CFD Simulation

4.5.1 Three Nozzle DS Simulation Geometry

In this case, two more nozzles were added to the geometry to account for the three DS nozzles. This can be seen in the Figure 4.19.

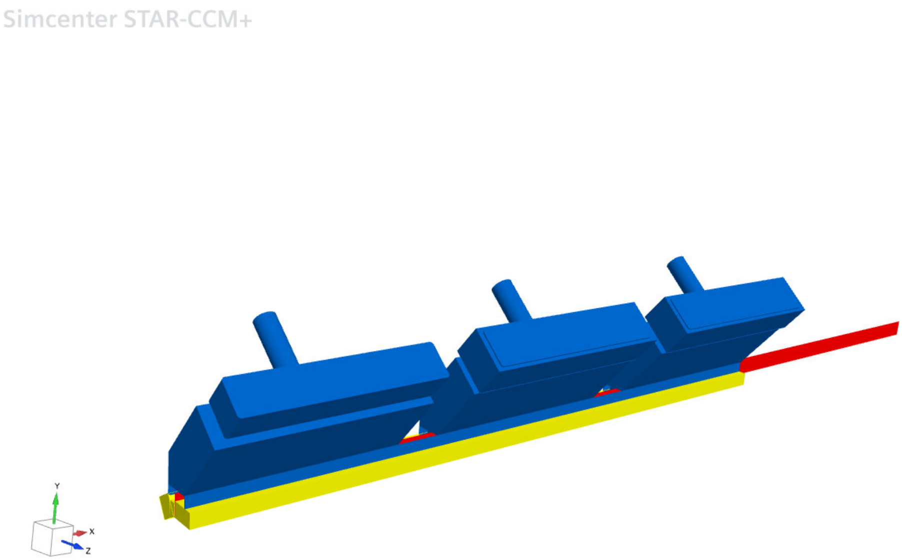

Figure 4.19: The three nozzle DS CAD geometry.

4.5.2 Region Definition and Set Up

In this simulation, only the regions for the packaging material and the surrounding air remain. When the flow within the nozzle is no longer solved, the resulting data at the nozzle outlets for the one nozzle DS simulation is extracted and then mapped to account for the flow existing in the nozzles. This methodology will result in a realistic simulation while minimizing computational time and resources. To do this, one has to first create a new XYZ table, in which the desired scalars are chosen, in this case the temperature, velocity and turbulent viscosity ratio at the nozzle outlets, which can be seen in the Figure 4.8 (the small yellow surfaces). This table is then imported into a new simulation with all three DS nozzles. The boundary condition at the nozzle outlets are now changed to a velocity inlet and the input data is the imported table.

4.5.3 Simulation Results Validating the Mapping of Results

In this section, the results of the simulation will be shown directly, to verify whether the data has been successfully mapped or not, two more 2D planes were added similar to the one seen in Figure 4.6. The results can be seen in Figures 4.20 and 4.21 and it shows that the mapped data is successfully accounting for all three nozzles, since there are identical flows at all three nozzles.

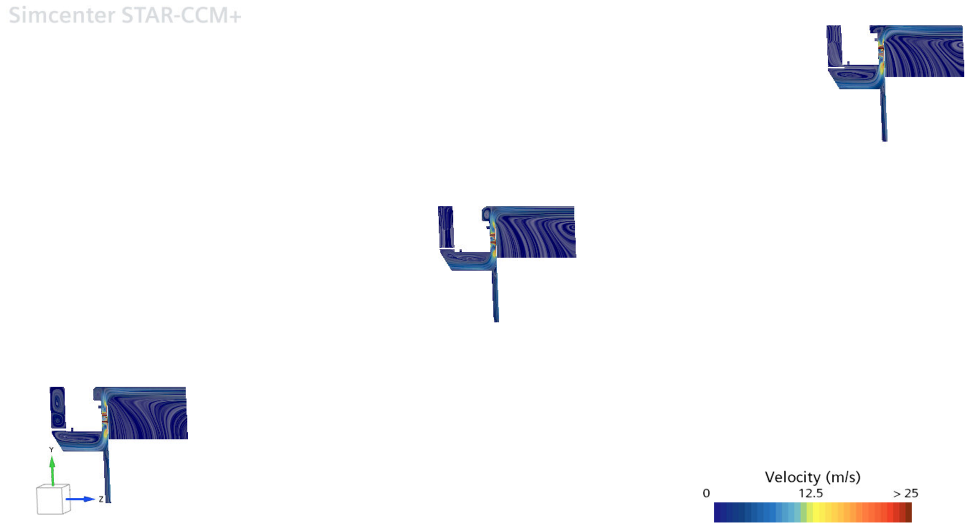

Figure 4.20: Velocity scene for the three nozzles for the three nozzles DS simulation, similar to the ones seen in Figure 5.4.

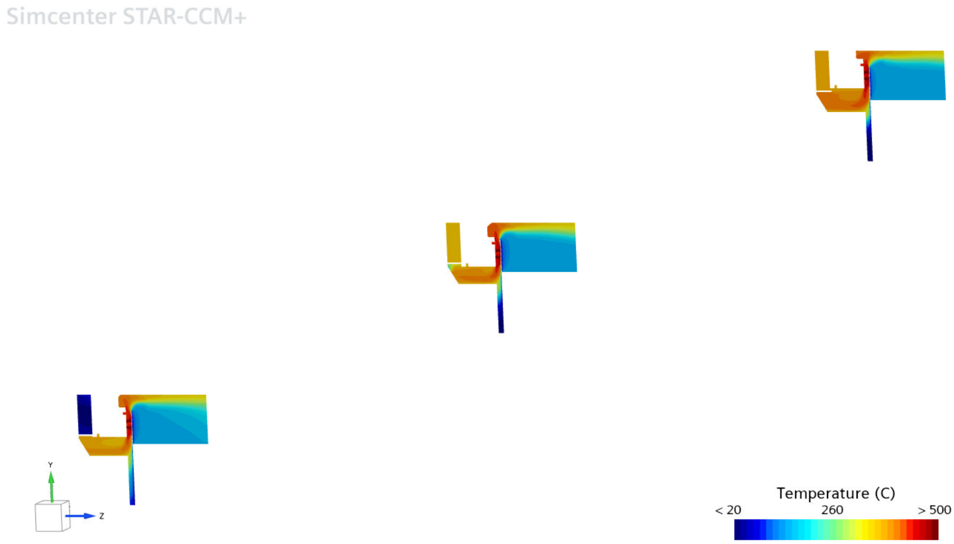

Figure 4.21: Temperature distribution for the three nozzle simulation, similar to Figure 5.6.

4.6 Two Nozzle OS CFD Simulation

4.6.1 Two Nozzle OS CFD Simulation Geometry

For this simulation, only one more nozzle is added, since there are only two nozzles on the operator side. The updated CAD geometry can be seen in Figure 4.22.

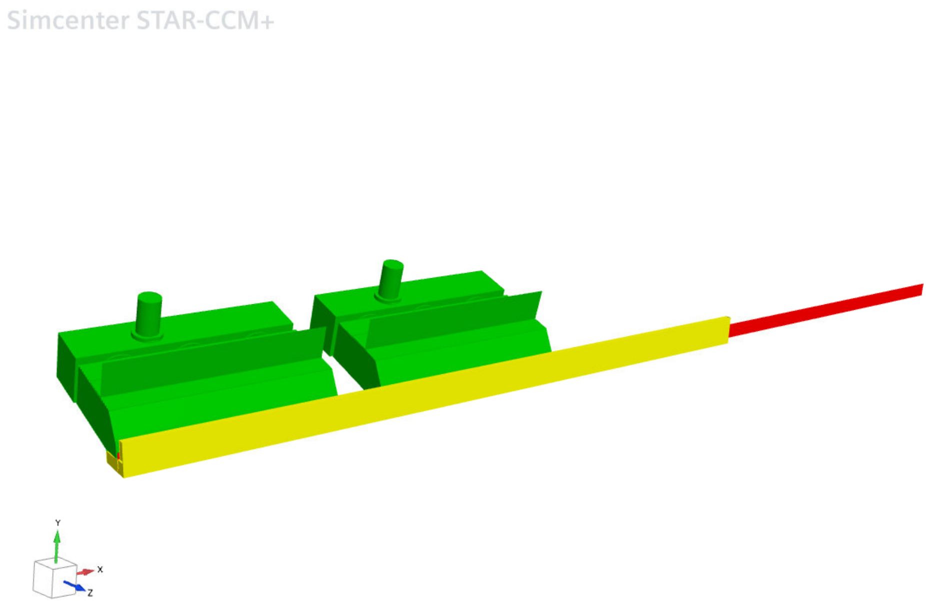

Figure 4.22: The two nozzle OS CAD geometry.

4.6.2 Region Definition and Set Up

For this case the same workflow is used as described in Section 4.5. The main goal of the simulations described in this and the previous section is to confirm that the mapping of the resulting data from the one nozzle simulations to account for multiple nozzles is accurate.

4.6.3 Simulation Results Validating the Mapping of Results

The mapped data were verified for the operator side. The velocity flow and temperature distribution behave as expected, see Figures 4.23 and 4.24.

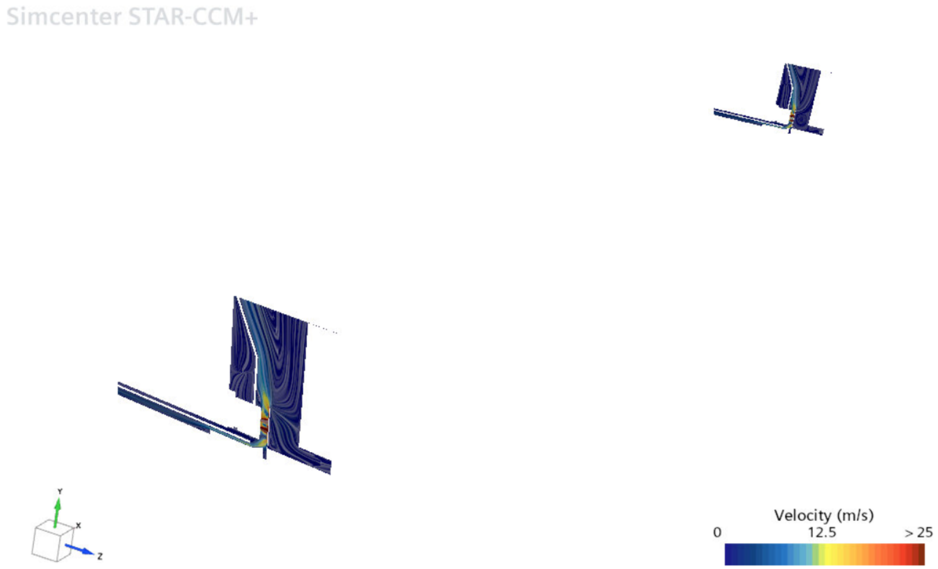

Figure 4.23: Velocity scene for the two nozzles, similar to Figure 5.8.

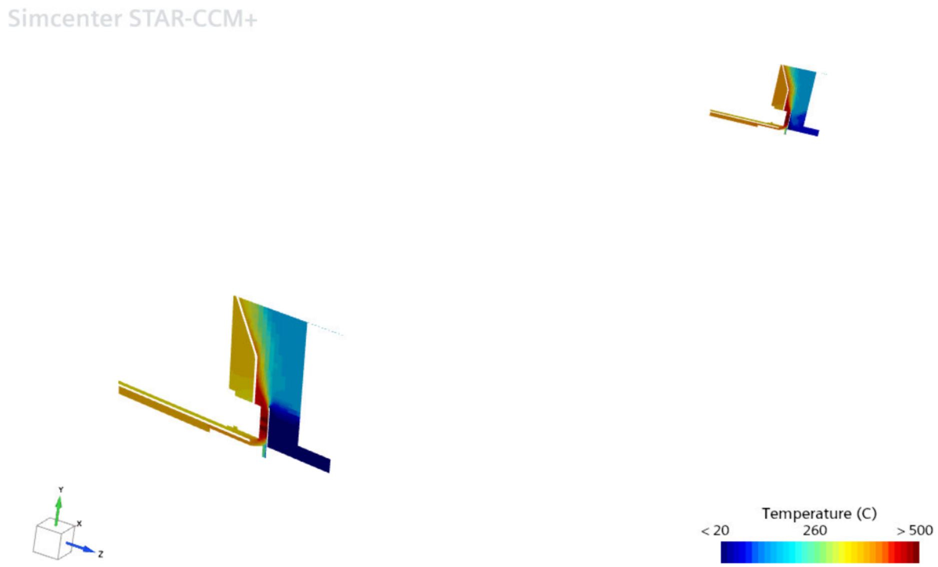

Figure 4.24: Temperature distribution for the two nozzles, similar to Figure 5.10.

4.7 The Final CFD model for the Reference Geometry

4.7.1 CAD Geometry for the Final CFD Simulation for the Reference Geometry

All five nozzles are now included in one simulation, the outer plate (yellow part) and the vacuum boxes (pink parts) are also added to the simulation. Blanks are defined as packaging material solid parts with gaps between them. The surrounding air region is expanded to account for the larger region of interest, all these modifications can be seen in Figure 4.25.

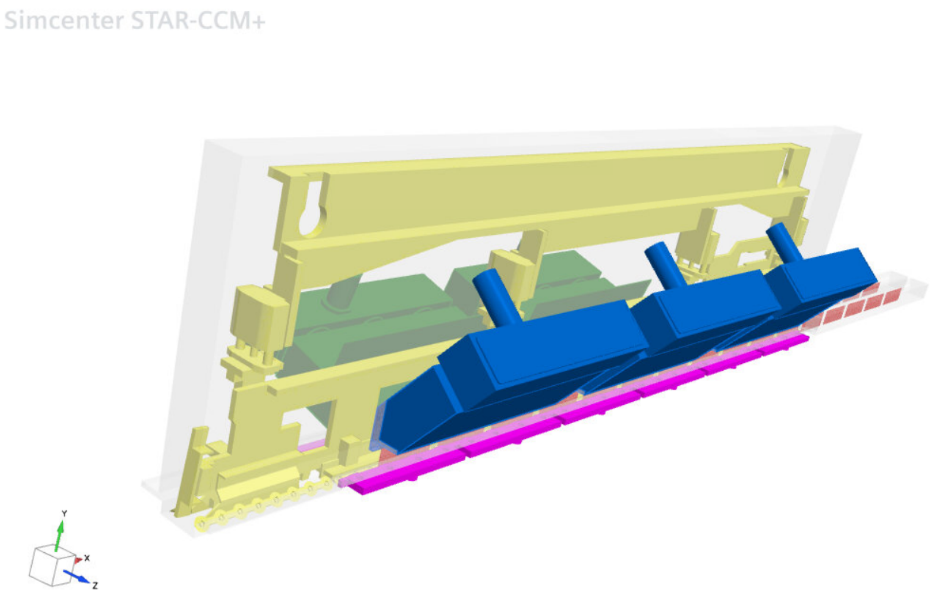

Figure 4.25: Updated CFD model.

4.7.2 Region Definition and Set Up

The physics continua for the outer plate is steel, see Table 4.2, and all the boundary conditions are wall. The vacuum boxes are also made of steel and the boundary conditions are also wall boundaries. The fluid domain within the vacuum boxes uses the air physics continua, see Table 4.1. In this domain, there are defined outlets, to lead the flow out of each box, otherwise the wall boundary is utilized. This is the CFD model that is used as a reference, which means that the concepts generated later will be directly compared to the results obtained from this model. Additionally, this setup will be used in the coming concept generation phase, a change is made to the geometry, and then the simulation is rerun to study the temperature on the outer plate.

4.7.3 Updated Mesh Settings

As one can see in Figure 4.25, the surrounding air region has been expanded significantly, this is to include the outer plate within the region. The nozzles are no longer meshed, since their data is mapped at their outlet. A coarser mesh size was tested, mainly to reduce the overall computational time, since after this simulation many new simulations would be created to test potential concepts. All mesh settings remained the same as before, but the base size was changed to 4 mm. This was deemed acceptable, since the overall temperature change on the outer plate was negligible, see Figure 5.19. This also resulted in a far lower simulation time. Regarding the mesh settings for the fluid region within the vacuum boxes, the same mesh settings that can be seen on Table 4.4 were applied, except for a 4 mm base size. The default mesh settings were defined for the outer plate, with a base size of 4 mm.

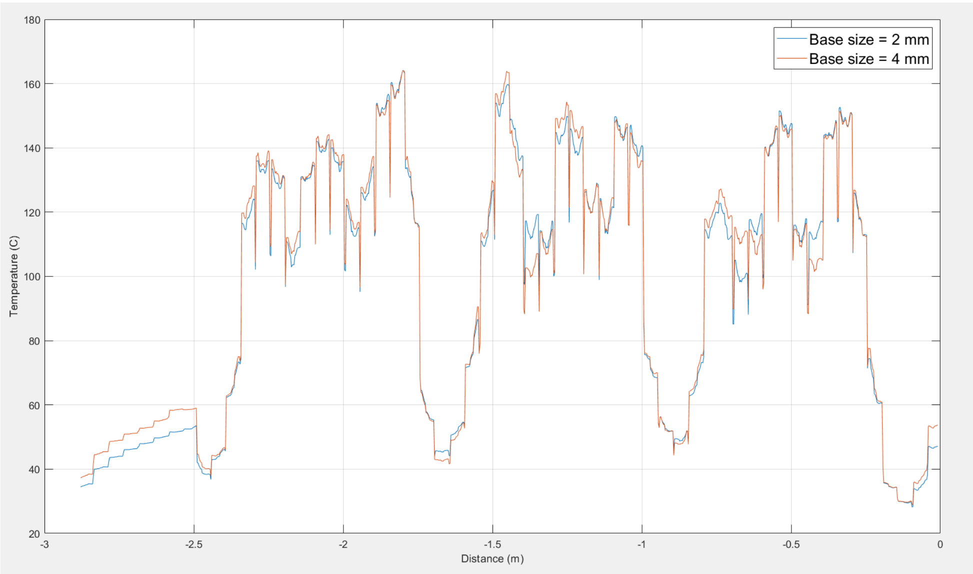

Figure 4.26: The resulting temperature for different base size of the mesh, the temperature is on the line probe that can be seen in Figure 5.19.

4.8 FEM Simulation Set Up

The mesh created during the CFD-simulation is exported as a case file, which is a file type that stores generated mesh data and field function data like temperature.

This case file is then imported into the FEM software. The chosen mesh type for the CFD-simulation is trimmed cell mesher, however this mesh type is not compatible with FEM-solvers. Therefore, once the CFD simulation is finished, the mesh type is changed to a tetrahedral mesher only for the outer plate. Star-CCM+ then interpolates the values to the new mesh type, without having to rerun the entire simulation. A change in the resulting temperature is observed when changing the mesh type, but is negligible in this case (1-2 degrees difference). The mesh for the FEM simulation can be seen in Figures 4.27 and 4.28.

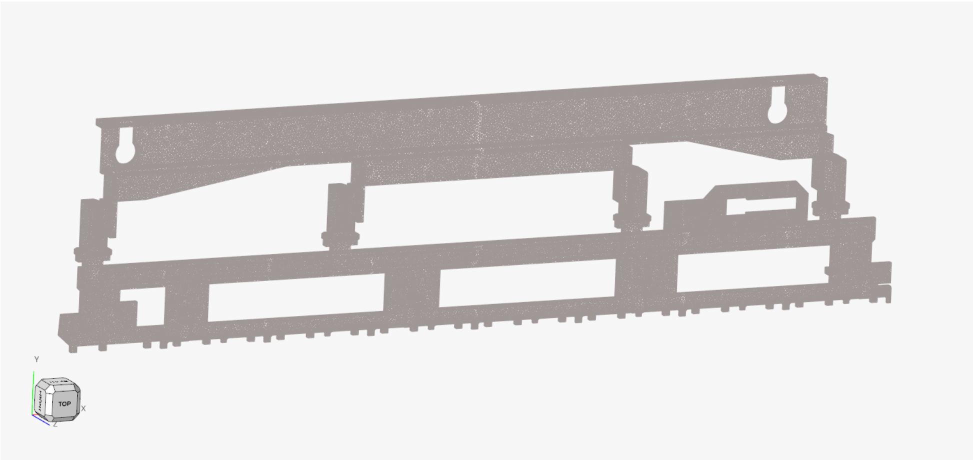

Figure 4.27: Mesh for the outer plate in Hypermesh.

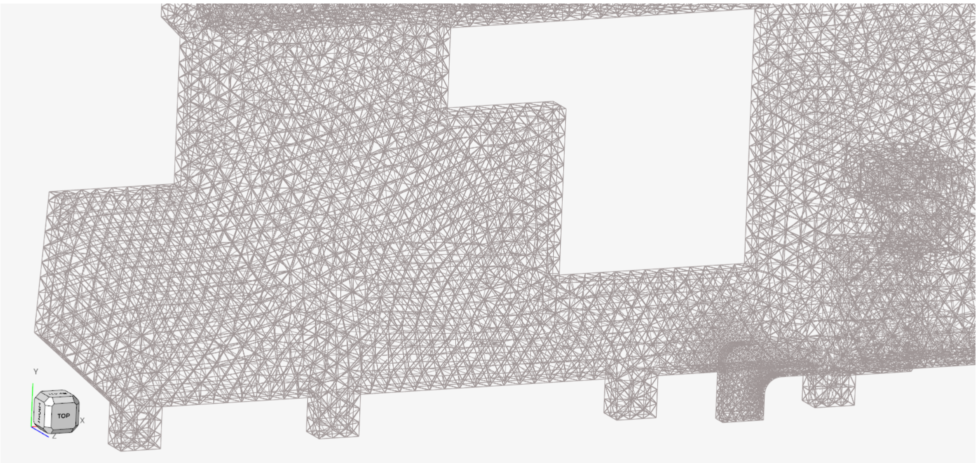

Figure 4.28: Zoomed in picture of the generated mesh in Hypermesh, showcasing the tetrahedral elements.

A fixed boundary condition was defined on the nodes that can be seen in the Figure

4.29, meaning that no displacement is allowed along the x,y,z-axis. The outer plate is bolted onto the main frame at these nodes, hence why movement is restricted. An additional boundary condition is the initial temperature of the outer plate, which is 20 degrees.

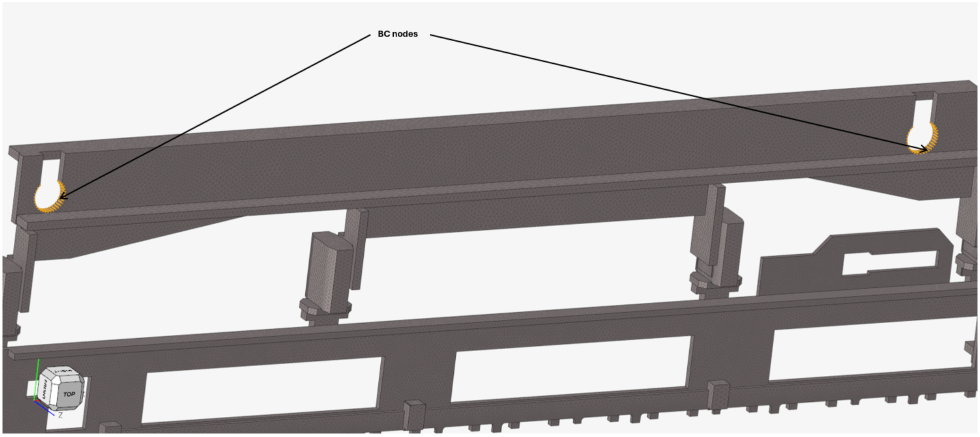

Figure 4.29: The nodes that are representing the boundary conditions (BC).

The resulting temperature field from Star-CCM+ on the outer plate was exported as a comma-separated value file (csv-file). The data extracted into the file are the positions of the coordinate, and its corresponding temperature. The csv-file was used as an input to an inbuilt field-operation, the temperature is then imported into HyperMesh as a temperature load. There are no prebuilt material parameters in HyperMesh, one must manually add that data to the software, typical steel and aluminum data are used in this case, see Tables 4.9 and 4.10.

Table 4.9: Defined values for the material steel in Hypermesh.

Property	Value
Thermal Conductivity [W/mK]	45
Specific Heat [J/kgK]	460
Zero Thermal Expansion [C]	20
Thermal Expansion Coefficient [1/K]	$1.2 \cdot 10^{-5}$
Density [kg/m^3]	7850
Young's modulus [GPa]	210
Poisson's ratio [-]	0.3

Table 4.10: Defined values for the material aluminum in Hypermesh.

Property	**Value**
Thermal Conductivity [W/mK]	167
Specific Heat [J/kgK]	897
Zero Thermal Expansion [C]	20
Thermal Expansion Coefficient [1/K]	$2.32 \cdot 10^{-5}$
Density [kg/m^3]	2700
Young's modulus [GPa]	68.9
Poisson's ratio [-]	0.33

5 Simulation results and discussion

In this section, the results will be presented. The validity of the results will be discussed, and whether a concept is robust or not.

5.1 Background and Intended Methodology to Validate Results and Discussion

A 2D plane at nozzle outlets was defined, to study various results, see the Figure 5.1. Plots were also generated, to extract and compare relevant data. Monitor plots were set up, for example for the mass flow inlet and outlet, to ensure that they are converging to the same value. The automatically generated residual plot from Star-CCM+ were also studied to validate whether the solution has converged.

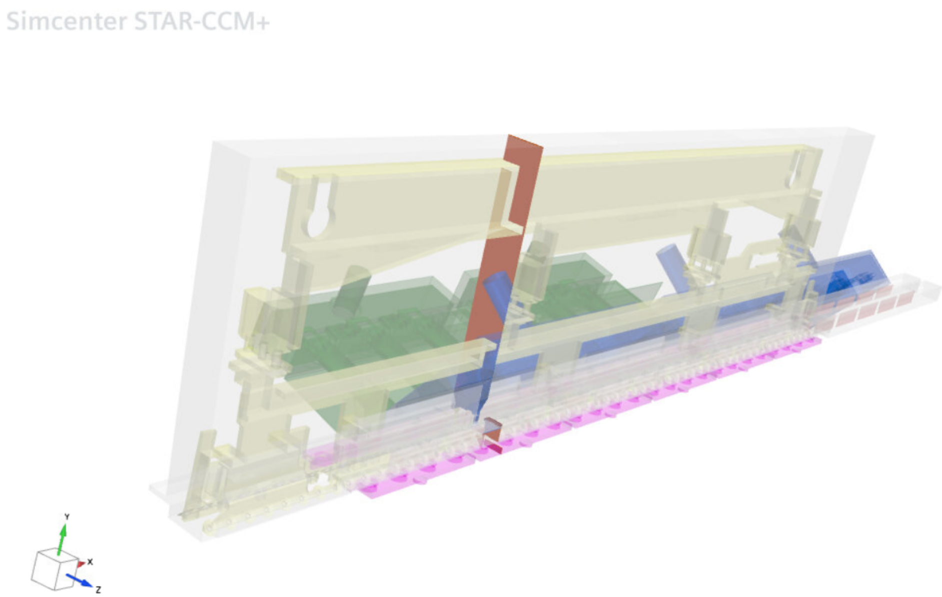

Figure 5.1: The location of the 2D plane.

5.2 One Nozzle DS CFD Simulation Results

The mass flow and the residual plot were studied to verify convergence. The mass flow plot can be seen in Figure 5.2, the plot shows that the solution is converged after approximately 1000 iterations. Henceforth, the number of iterations that the simulations will run is 1000, not the default 2000. From now on the mass flow plot and the residual plot will not be presented, since they are very similar for all the simulations.

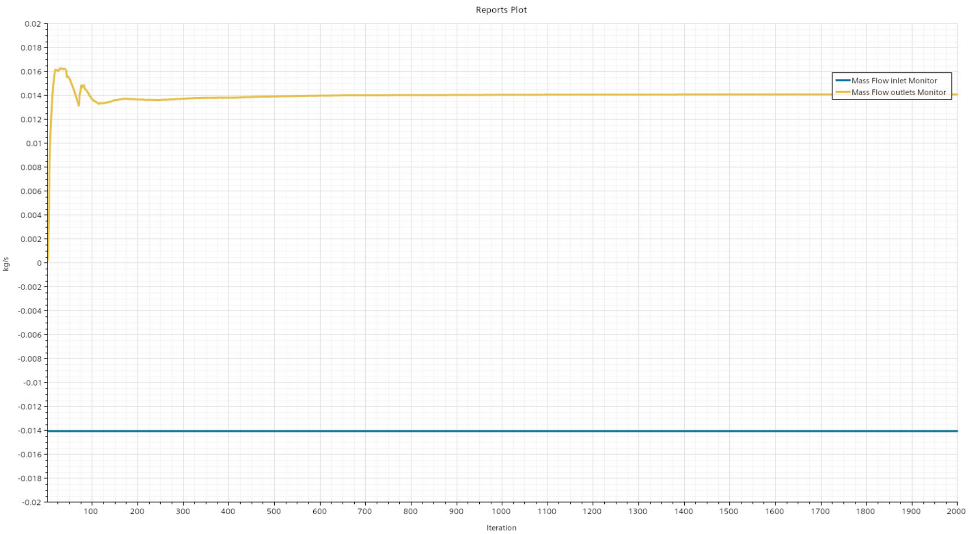

Figure 5.2: Mass flow inlet and outlet plot for the DS.

The residual plot can be seen in Figure 5.3, the residuals have dropped and are stable, which is the desired outcome. Scenes were also studied to analyze the flow behavior and the calculated values were stable, the relevant scenes can be seen in Figures 5.4-5.7.

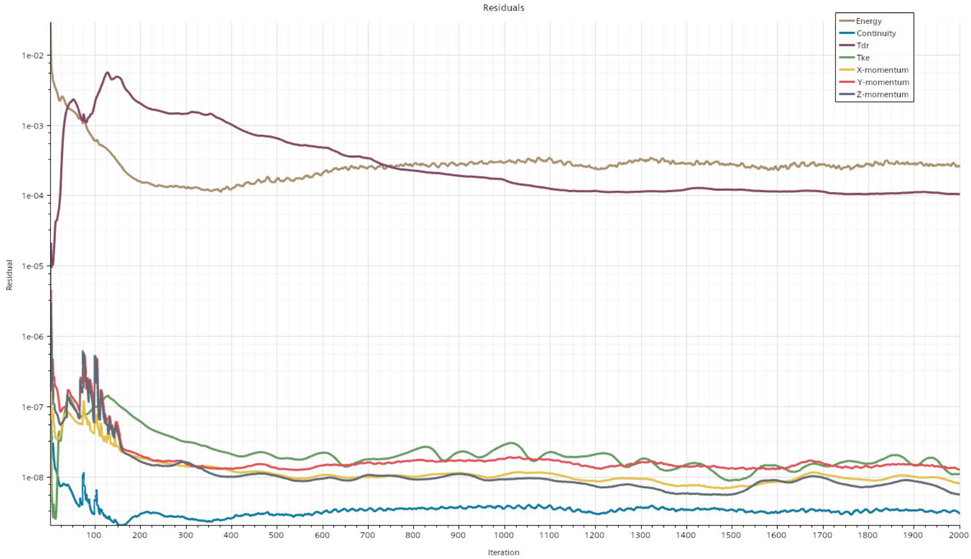

Figure 5.3: The residual plot generated by Star-CCM+.

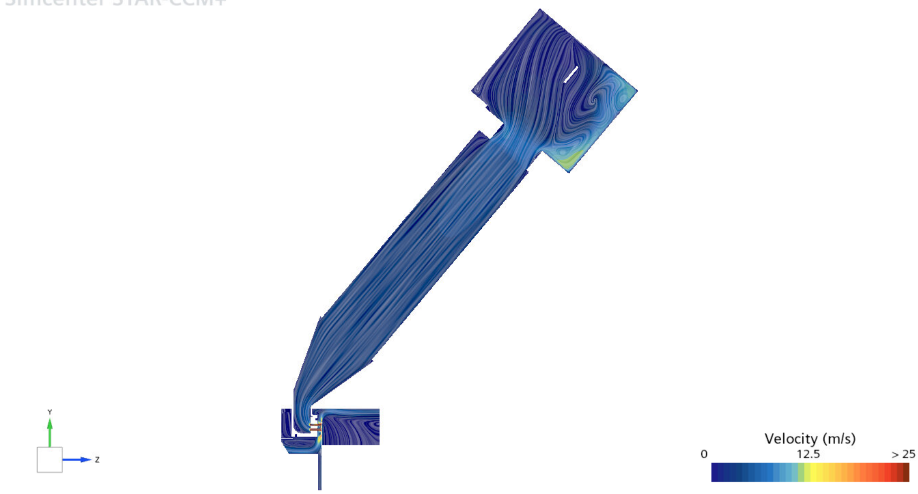

Figure 5.4: The resulting velocity for the DS simulation.

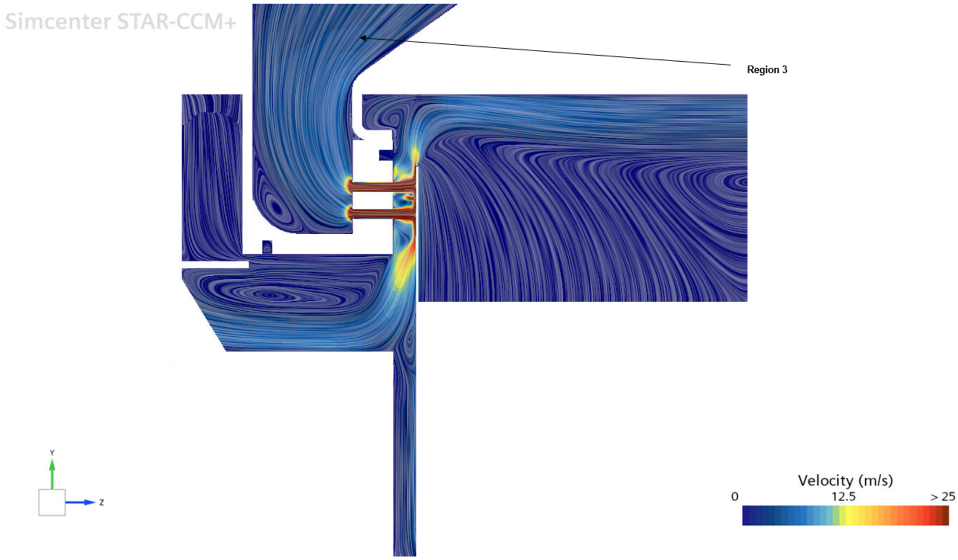

Figure 5.5: A zoomed in picture to visualize the velocity at the outlet for the DS simulation.

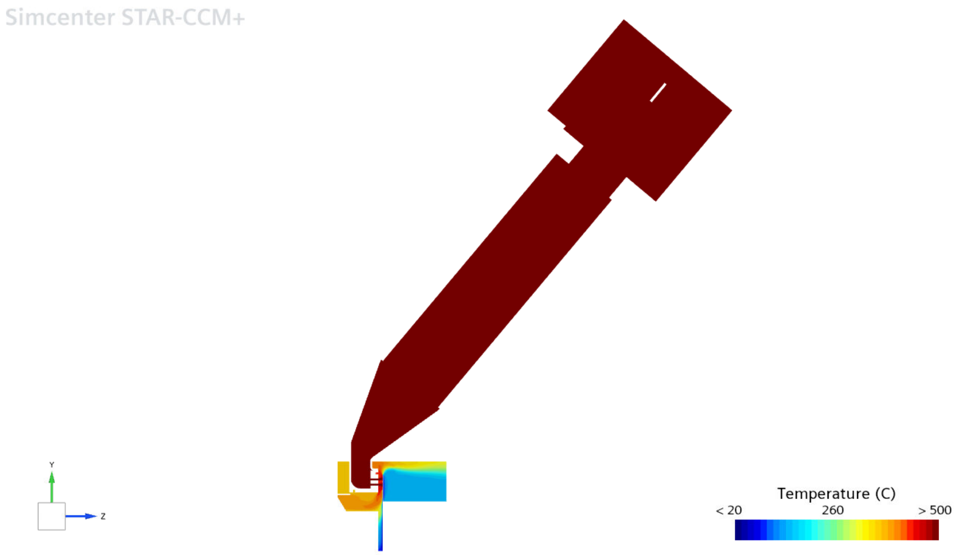

Figure 5.6: The resulting temperature distribution for the DS simulation.

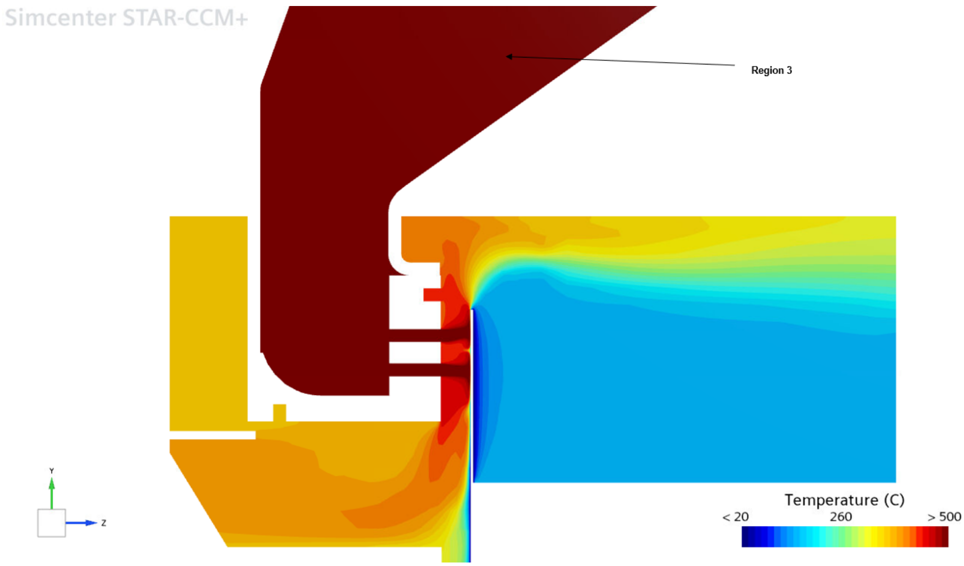

Figure 5.7: Zoomed in figure to enhance the visualization of the temperature distribution for the DS simulation.

5.3 One Nozzle OS CFD Simulation Results

The relevant results for this simulation can be seen in the Figures 5.8-5.11. Nothing that appears out of the ordinary, the overall simulation results is as expected.

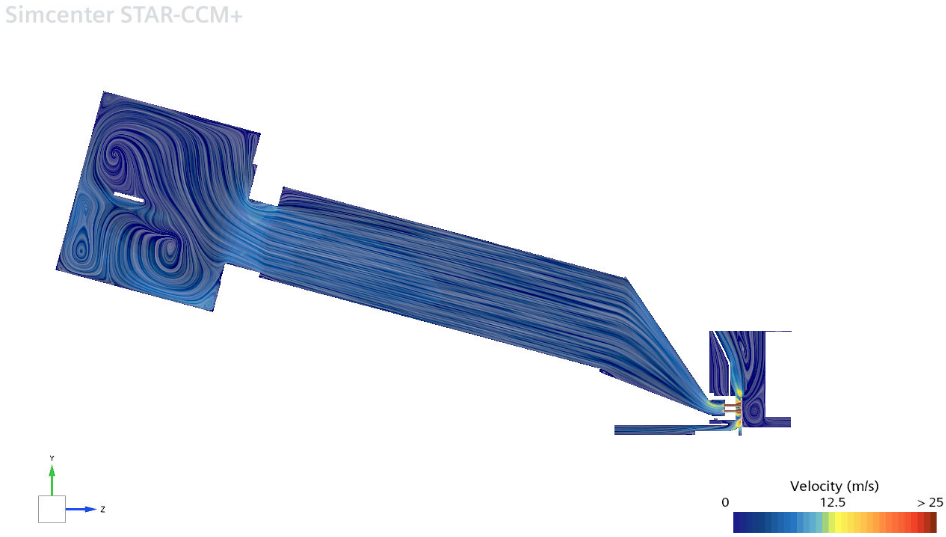

Figure 5.8: The resulting velocity scene for the OS simulation.

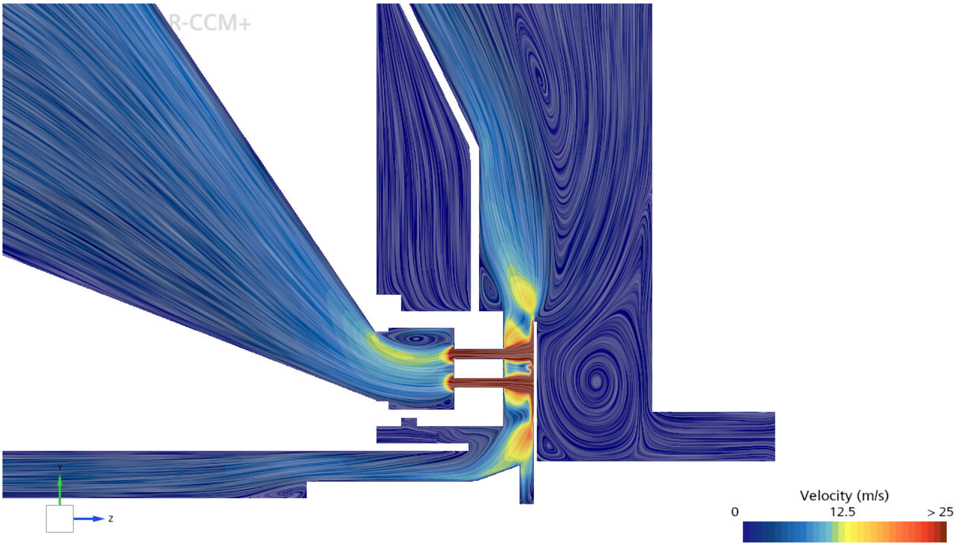

Figure 5.9: Zoomed in figure to help visualize the velocity at the outlet for the OS simulation.

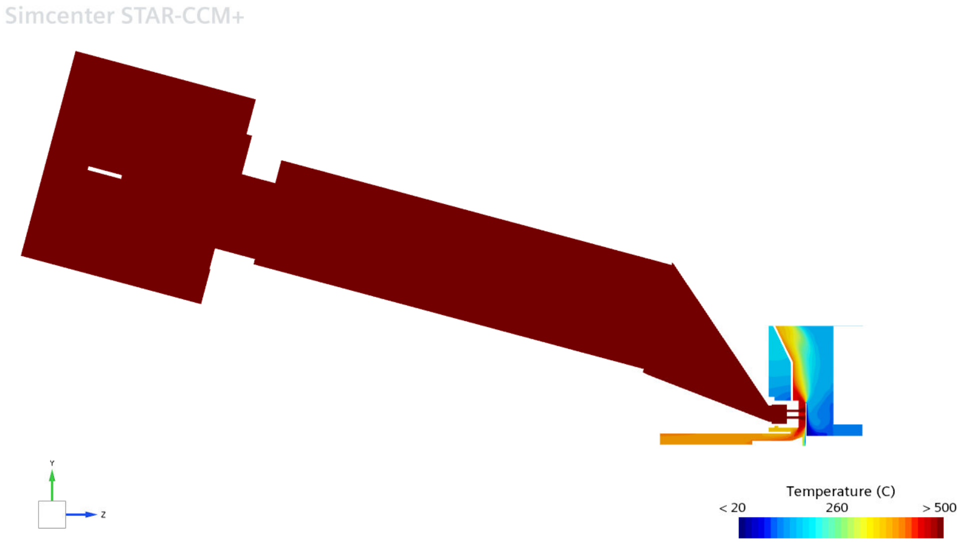

Figure 5.10: Resulting temperature field for the OS simulation.

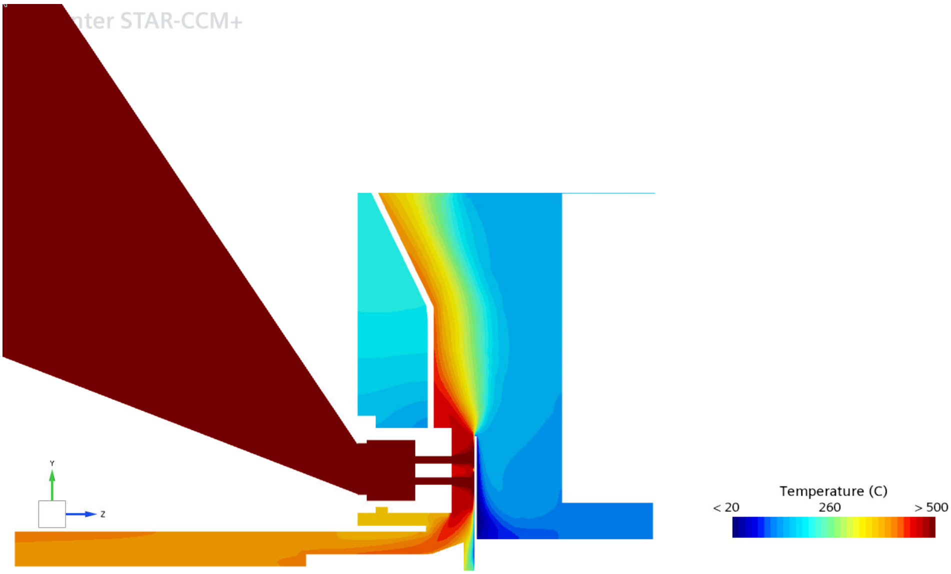

Figure 5.11: Resulting temperature field for the OS simulation, zoomed to better visualize the temperature distribution at the nozzle outlet.

5.4 Reference Geometry Simulation Results

For the simulation with all five nozzles, the vacuum boxes and the outer plate, the mass flow and residual plots are also converging. The velocity and temperature distribution are shown, see Figures 5.12 and 5.13. The cooling channels attached to the outer plate can also be seen in the figures below.

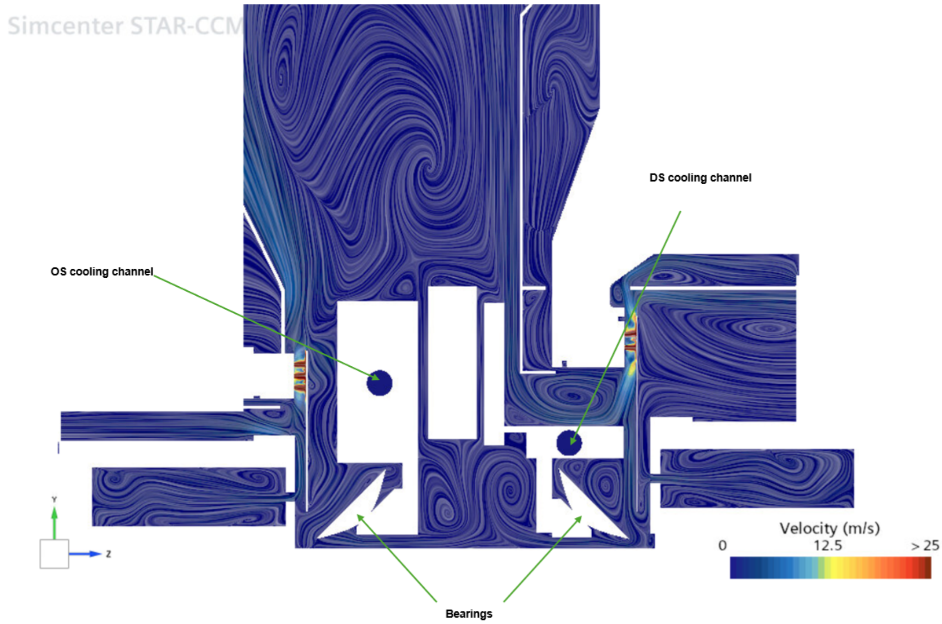

Figure 5.12: Velocity scene for the reference case.

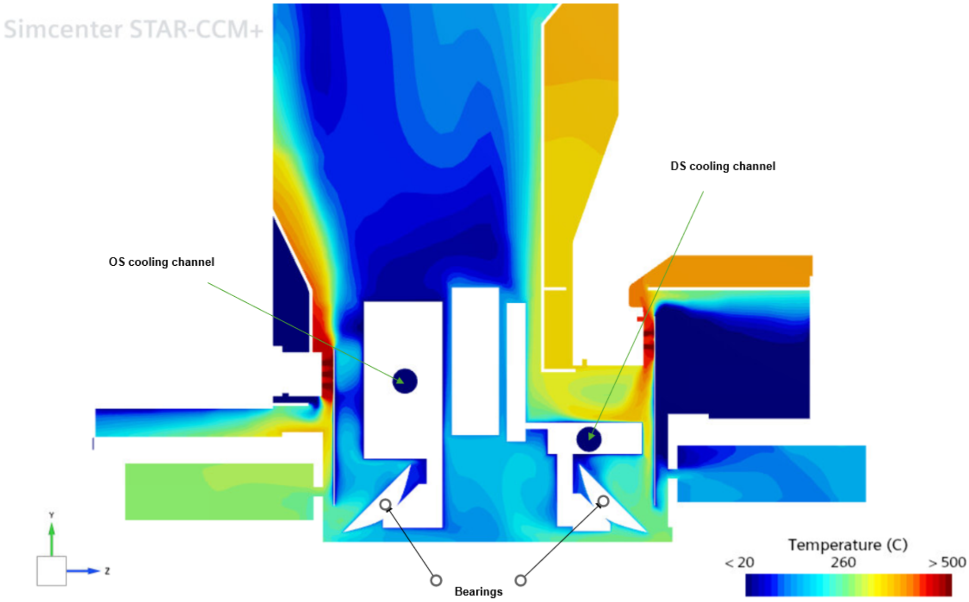

Figure 5.13: Temperature distribution for the reference case.

A new 2D plane was also created to visualize the velocity and temperature distribution in the gap between the blanks. The location of the 2D plane can be seen in the Figure 5.14. The resulting velocity and temperature scenes can be seen in the Figures 5.15 and 5.16. As expected, the distribution is different, since no PM exists in the defined plane, from the OS side the air is flowing straight onto the os cooling channel. For the DS side, the hot air is flowing out of the side sealer. The difference in flow properties in the Figures 5.12 and 5.15 shows that the results are reasonable. Mainly, since the airflow is expected to flow around the blanks and in the areas where there are no blanks the air flows through.

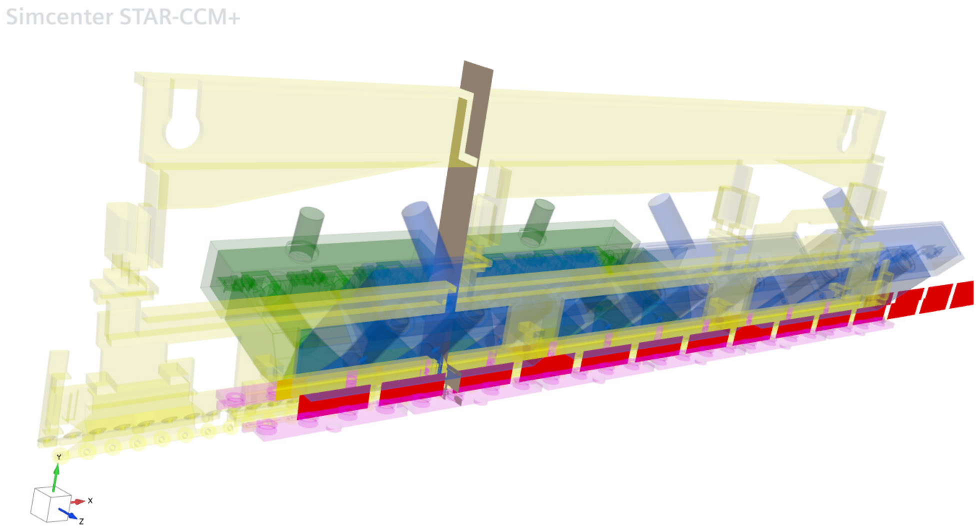

Figure 5.14: The newly defined 2D plane.

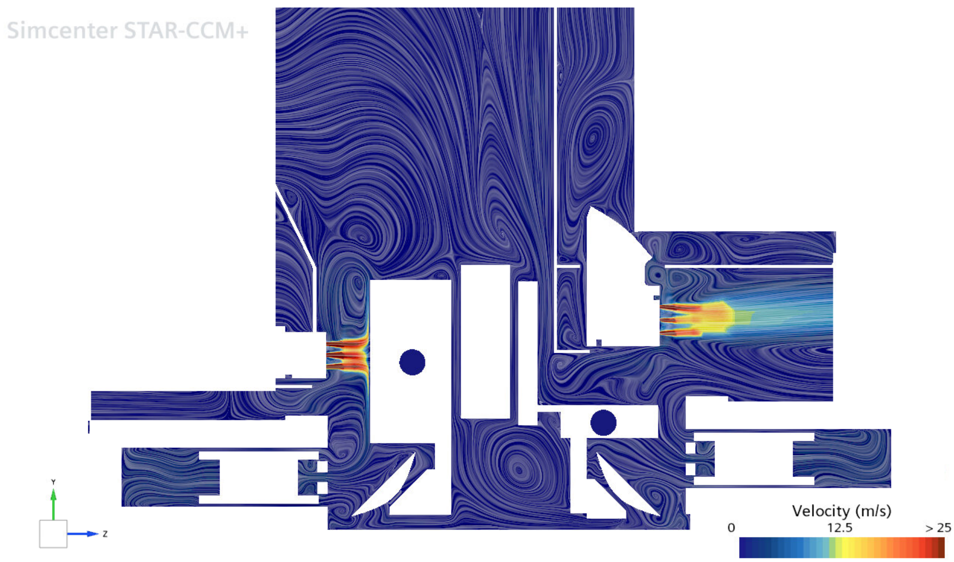

Figure 5.15: Velocity distribution where there is a gap between the PM.

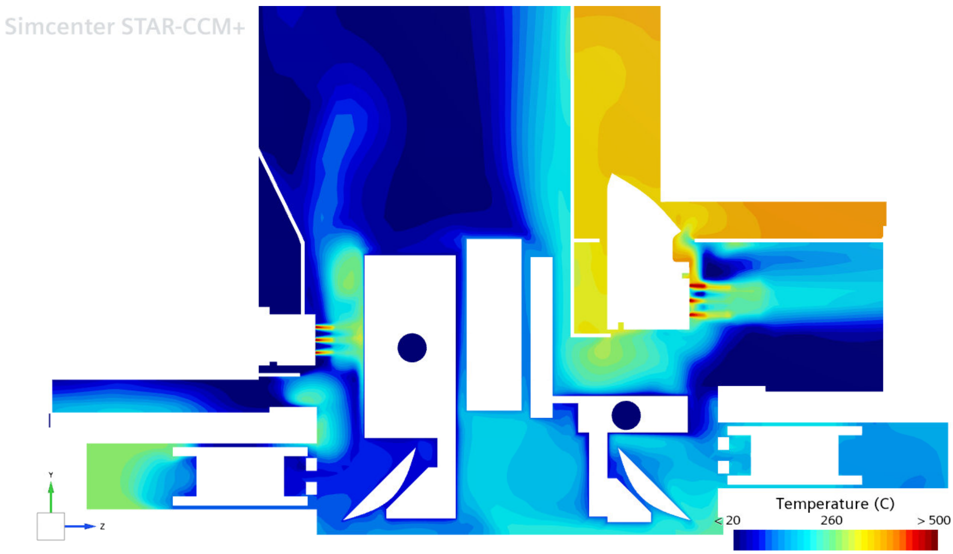

Figure 5.16: Temperature distribution where there is a gap between the PM.

Furthermore, an additional temperature scene was created solely for the outer plate since it is the mechanical part of interest in this thesis. The resulting temperature on the outer plate that can be seen in Figure 5.17 is imported into the FEM software as a thermal load. The resulting thermal deformation can be seen in Figure 5.18. Due to these results, the problem is now identified. The outer plate deforms over 2 mm in the Z-axis and the distance to the PM is approximately 2 mm, this might cause the production to halt when the plate is thermally expanded. This resulted in a clear goal of what the new concepts had to achieve to be deemed an acceptable solution, that the deformation in the Z-axis is less than 2 mm.

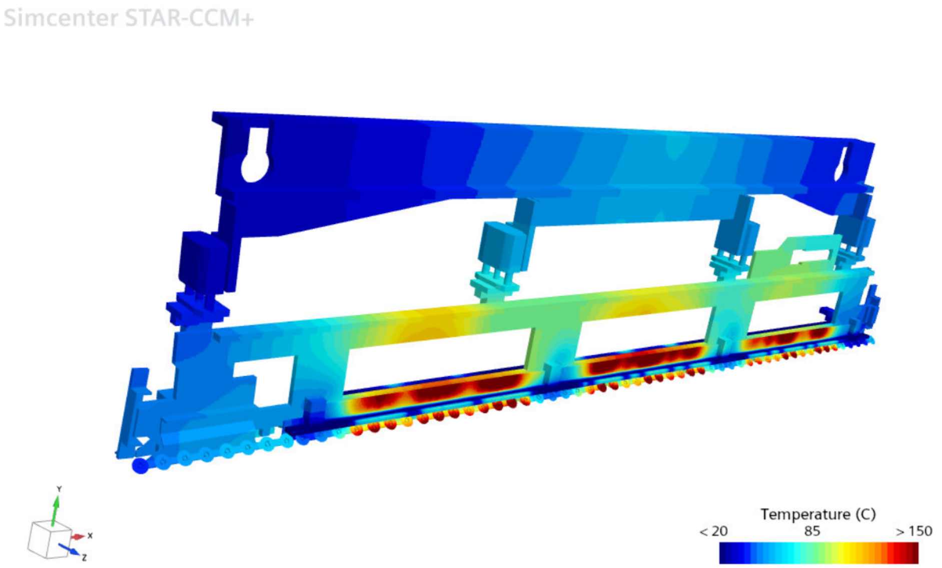

Figure 5.17: Temperature field on the outer plate.

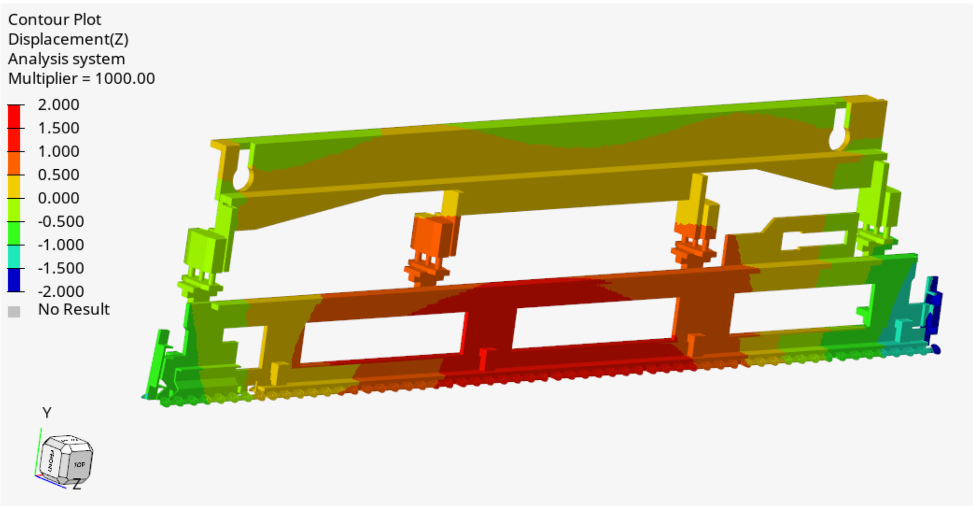

Figure 5.18: Resulting thermal deformation on the outer plate.

From the CFD simulation, one can extract data, for example, the temperature along the outer shell of the DS bearings. This can be done by defining a line along the bearings, see Figure 5.19 and then creating a plot, see Figure 5.20. This is one of many advantages of using simulation tools for different types of processes. This helps to better understand the process in great detail and visualize certain parts that are often hidden. In addition, these tools can be of great assistance optimizing structures and visualize the impact on the process.

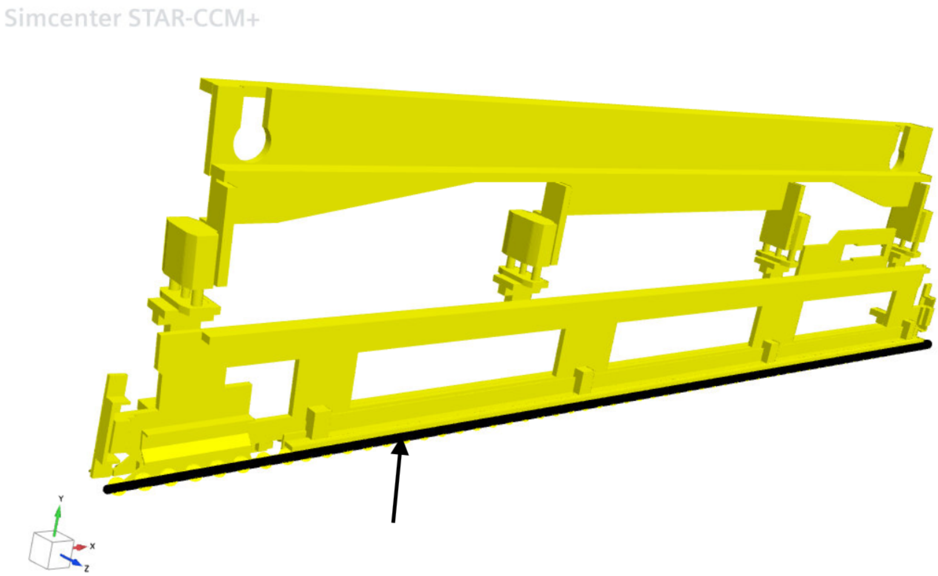

Figure 5.19: Line probe on bearings.

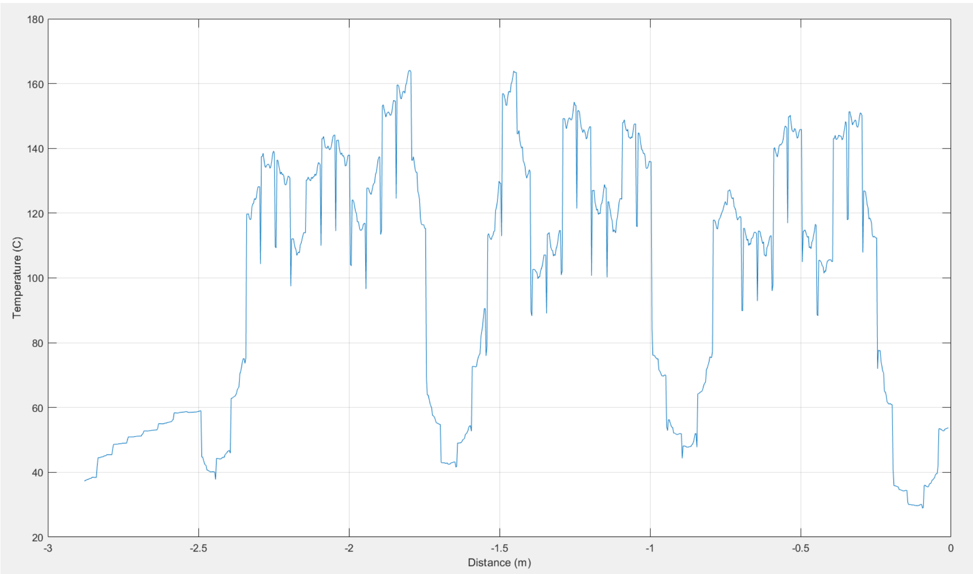

Figure 5.20: The temperature on the outer part of the bearings, data obtained from Star-CCM+ and then plotted using MATLAB.

5.5 Concept 1: Strategic Cut

Since high temperatures were observed in relatively small regions, this concept delved into minimizing the overall rigidity of the outer plate in the very hot regions and enable the plate to expand more freely. In the CAD geometry, three small cuts were made, see Figure 5.21, with the intention of making the plate less stiff and to allow the plate to deform into itself, resulting in lower deformations. The flow simulation converged based on the mass flow and residuals plot. The solved temperature on the outer plate can be seen in Figure 5.21. The resulting thermal deformation can be seen in Figure 5.21, it is clear that this solution is not robust, since the deformations are higher than 2 mm, and is therefore not considered any further.

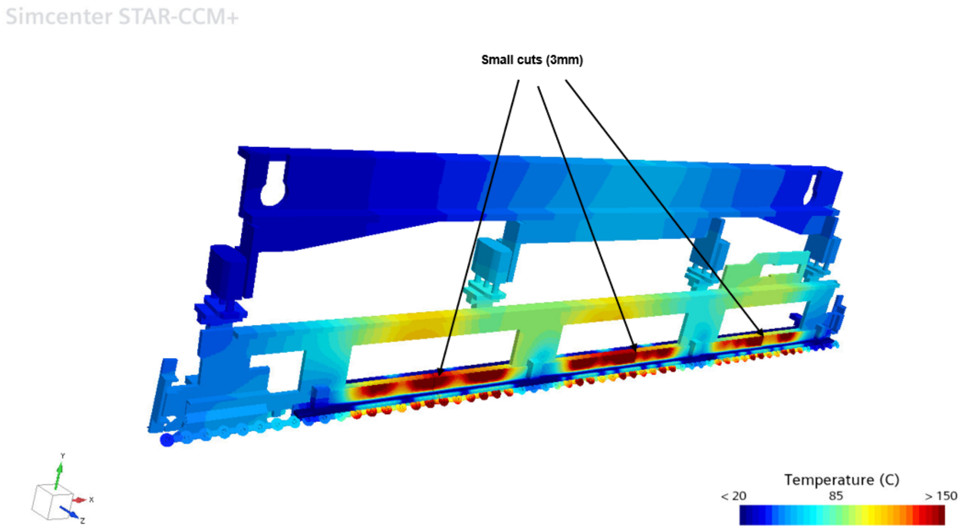

Figure 5.21: Temperature distribution for concept 1.

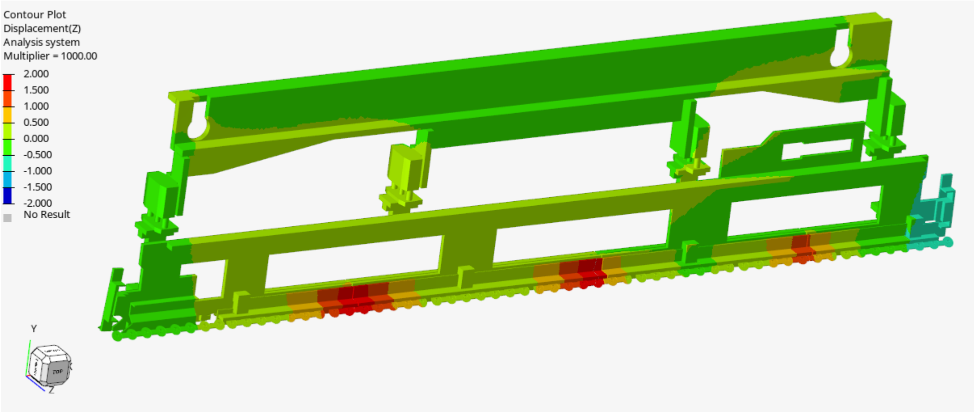

Figure 5.22: Temperature deformation for concept 1.

A plot is created for the deformations that exist on the line seen in the Figures 5.23 and 5.24, to compare the resulting thermal deformation of the concepts to the reference geometry. In the Figure 5.25, the generated plot can be seen and it is clear that the deformation exceeds 2 mm. The values on the Y-axis are not included, due to it being classified information.

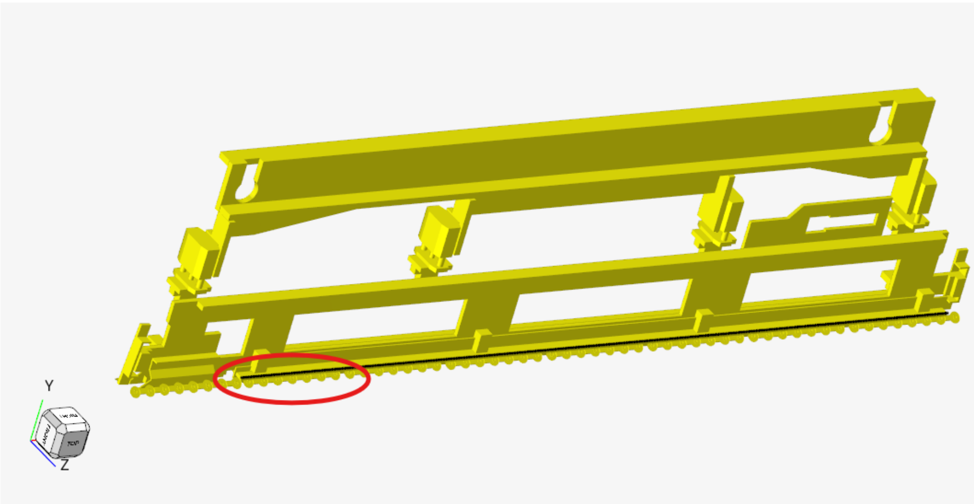

Figure 5.23: The location of the probe line in which a plot will be generated from.

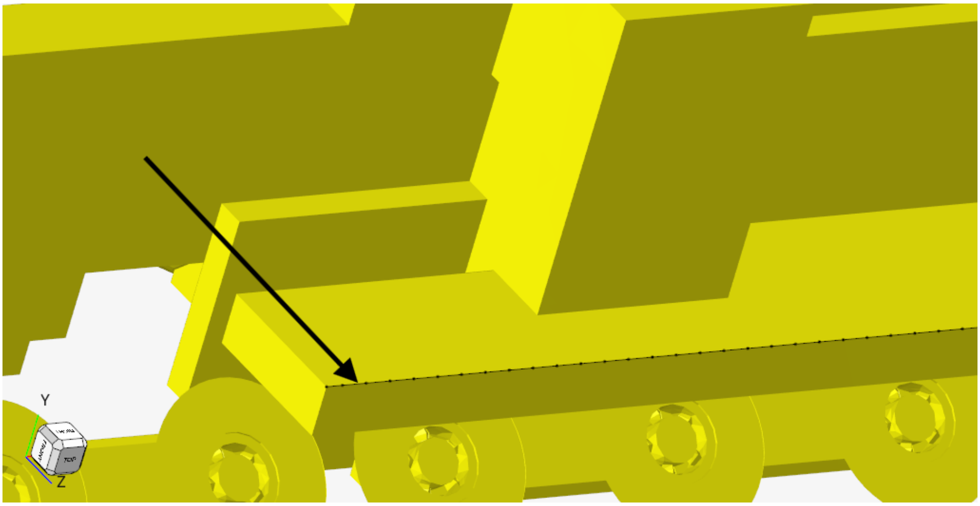

Figure 5.24: The location of the probe line in which a plot will be generated from, but now zoomed to better see its location.

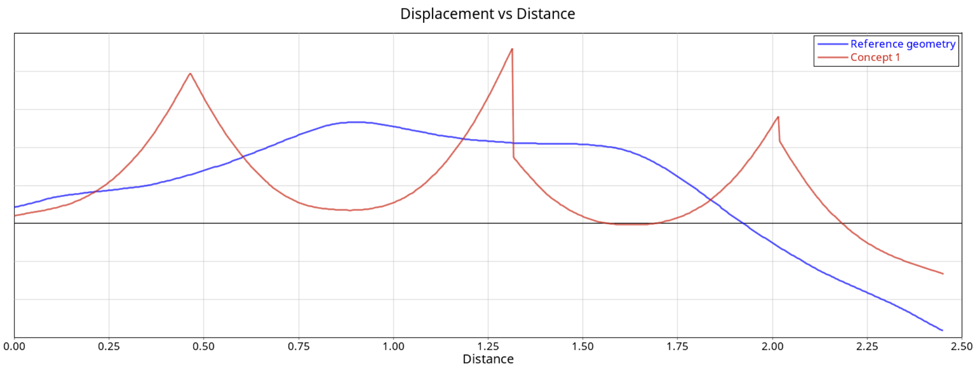

Figure 5.25: The deformation on the line that can be seen in the Figures 5.23 and 5.24.

5.6 Concept 2: Material Change

The second concept is to keep the current design of the outer plate, but change the material from steel to aluminum. The thermal conductivity of aluminum is more than ten times better compared to stainless steel [15]. This makes it a very interesting case to study, both to solve the current problem and to study the potential of incorporating aluminum for similar projects in the future. The CFD simulation converged and the temperature of the outer plate can be seen in Figure 5.26, the outer plate is cooler compared to the reference geometry as expected. Figure 5.27 shows the thermal deformation for this case study, and is also less than 2 mm, making this a potential solution.

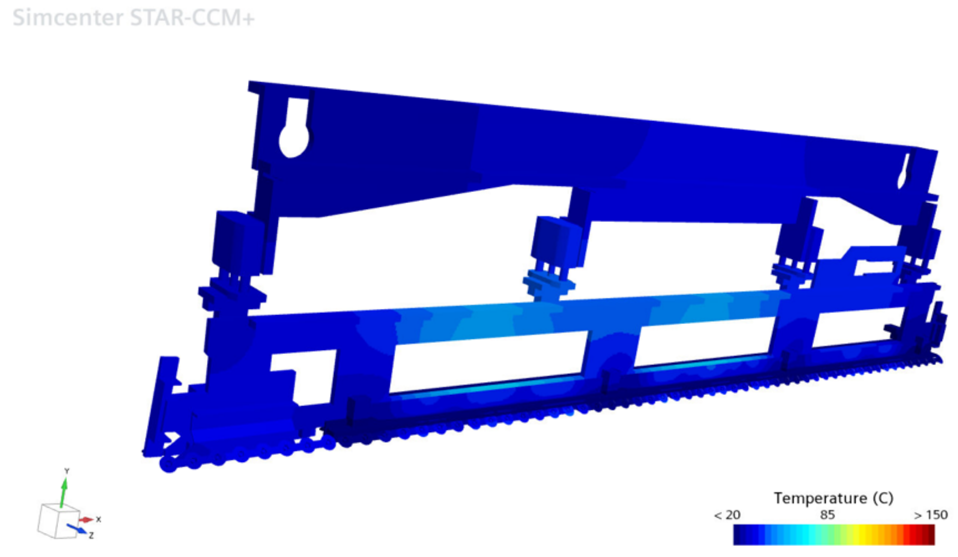

Figure 5.26: Temperature distribution for concept 2.

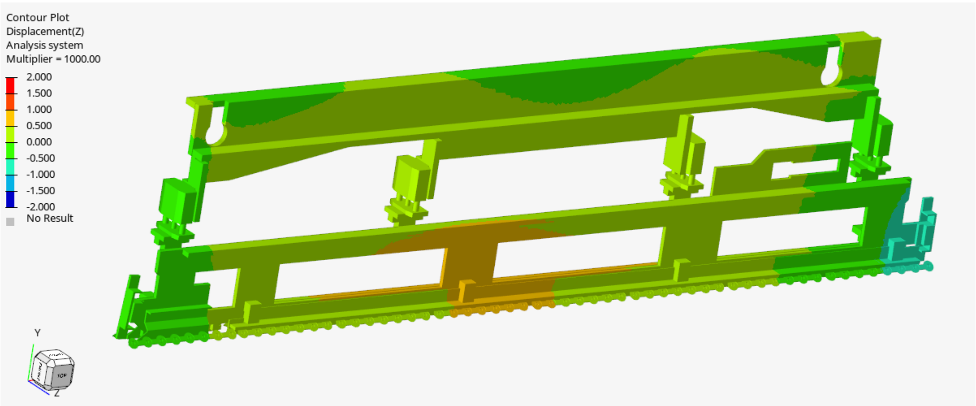

Figure 5.27: Thermal deformation for concept 2.

To compare concept 2 with reference geometry using actual data rather than scenes, the resulting deformation at the line previously seen in the Figures 5.23 and 5.24 can be seen in the Figure 5.28. It can be seen that concept 2 is a very promising solution that can be utilized for this specific project or for future projects that are similar.

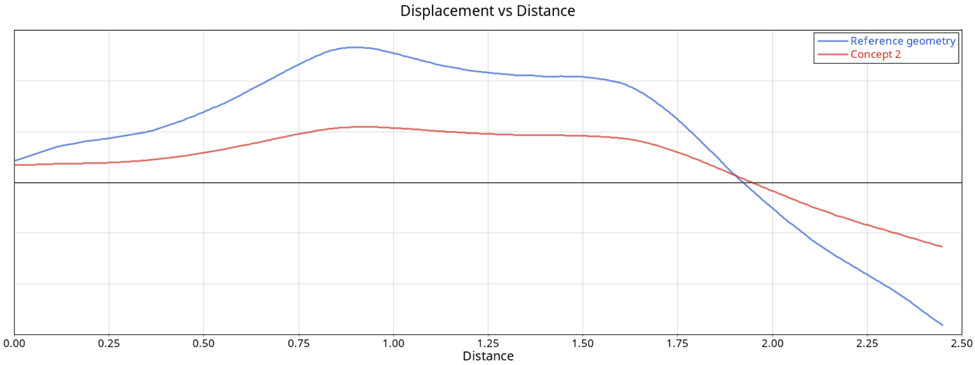

Figure 5.28: Deformation on the line in the Figures 5.23 and 5.24.

5.7 Concept 3: Beam Reinforcement

The resulting thermal deformation presented in Section 5.4 indicates that the problem arises due to the high deformations in the middle section. The main deformation is alongside the Z-axis, therefore an idea is to place a beam at the opposite side to even out the deformations. The necessary CAD changes were made, and the simulations were rerun and converged. The temperature on the outer plate can be seen in the Figure 5.29. The deformation in the Z axis is mainly due to uneven heating of the plate, hence if one were to place the beam on the side that is colder and let it heat up, it would evenly distribute the deformations. This assumption was confirmed with the results of the FEM simulation, Figure 5.30. Concept 3 is therefore a very practical solution to the current problem.

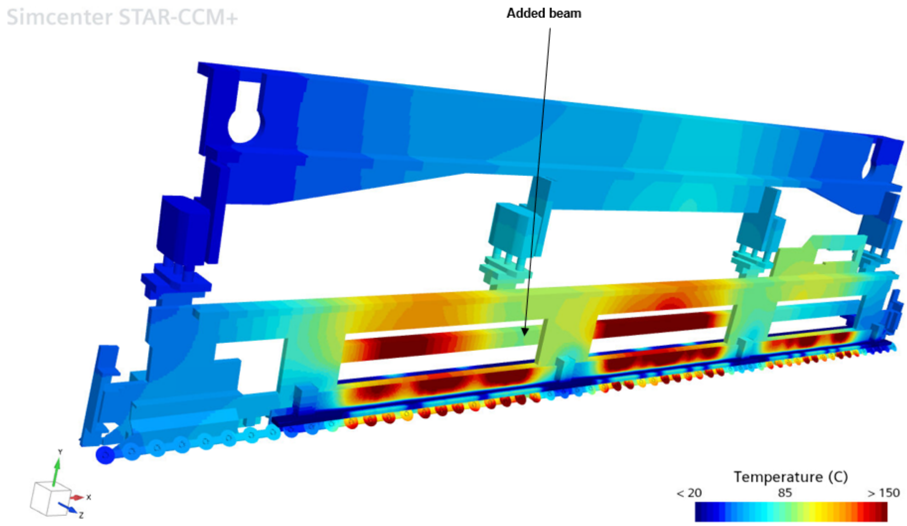

Figure 5.29: Temperature distribution for concept 3.

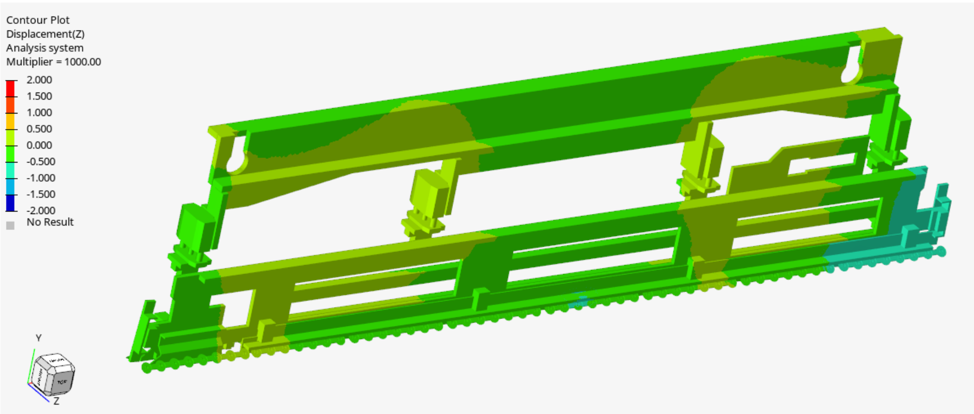

Figure 5.30: Thermal deformation for concept 3.

Like the previous cases, this concept was directly compared to the reference geometry by looking at the resulting deformation on the lines in the Figures 5.23 and 5.24. In Figure 5.31, the displacement plot can be seen and this concept appears to be a very robust solution to the current and future similar problems.

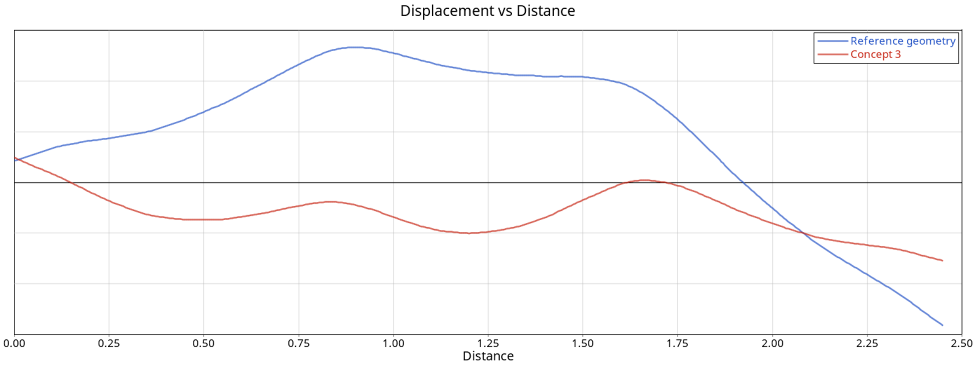

Figure 5.31: The resulting deformation that is present on the line that is in the Figures 5.23 and 5.24.

To further prove that the resulting thermal deformation in the Z-axis is due to uneven heating of the plate and not necessarily due to the structural rigidity, an additional simulation was made. In this case instead of having one beam added only on the OS, this time two beams were used, one for the OS and one for the DS, see Figure 5.32. In Figure 5.33, the resulting thermal deformation for the case of two beams can be seen and compared directly to the results of the reference geometry. It is clear that simply adding more beams with the intention of improving structural integrity will not solve the underlying issue, but instead decrease the robustness of the current outer plate. A solution is to therefore add a beam that has a appropriate location, like the one presented in concept 3.

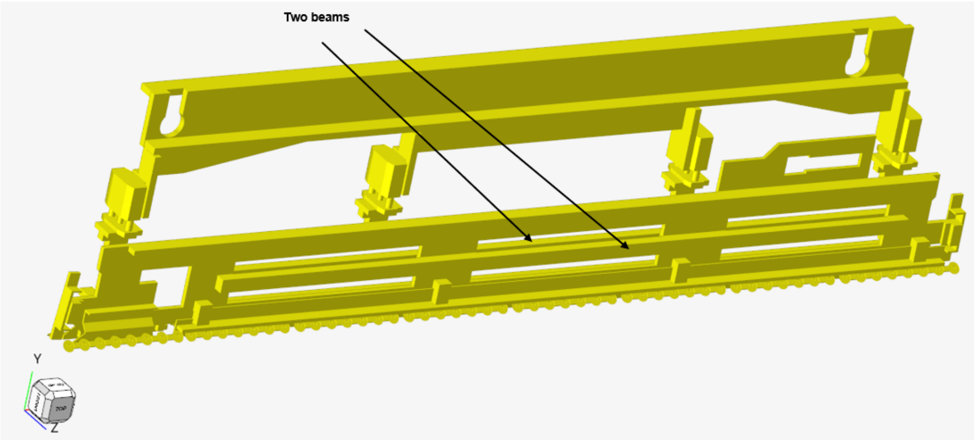

Figure 5.32: The case in which two beams were added instead of one.

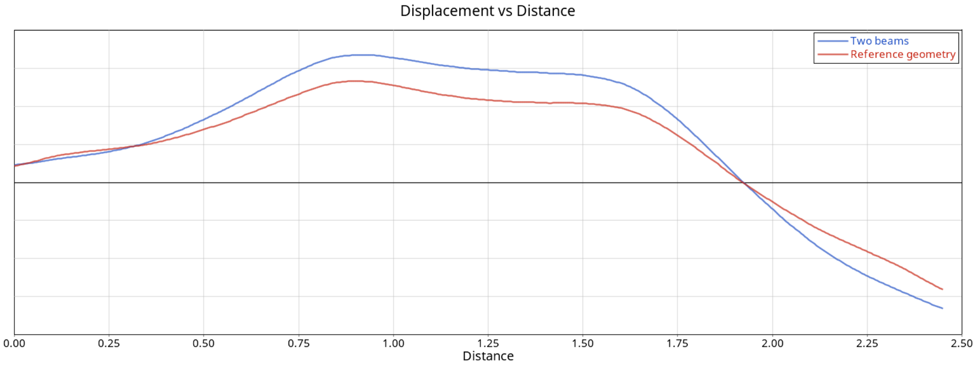

Figure 5.33: Deformation on the line in Figure 5.23 and 5.24 for the two beams scenario.

6 Overall Discussion and Future Work

In this section, an overall discussion regarding the work done in this thesis will be presented. The remaining work for each concept will be described.

6.1 Scientific Contribution and Source of Error

In general, the workflow utilized in this thesis to obtain the overall production flow for the side sealer can be used in similar industrial machines and will result in an accurate model. The generated model can be used to solve a wide variety of problems in existing industrial equipment. It can also be used early in the product development process to quickly identify potential problems. This can be done by Tetra Pak or other companies as well. However, it is of great importance that one studies the equipment to be simulated well enough to decide on the options seen in Sections 4.2 and 4.3. For example, if the flow is more complex than the one studied in this project, then perhaps one needs to use an unsteady solver or a different mesh type, to ensure that no important details are missed. In simulations, it is often hard to identify and objectively decide the options presented in Sections 4.2 and 4.3 and is the main source of error in this thesis.

6.2 Concept 1 Discussion and Future Work

The first concept does not solve the problem studied in this thesis, however it minimizes the temperature deformation at the end of the outer plate, when compared to the reference geometry. The problem that remains unsolved is that the thermal deformation in the middle of the plate is more than 2 mm, one could further develop this concept and add elements to the design that minimize the thermal deformation in the middle. In addition, one would need to make sure that by cutting the outer plate, future problems will not arise, in theory, this would be the most cost-effective solution if it were applicable.

6.3 Concept 2 Discussion and Future Work

For the second concept, while not necessarily the recommended solution for this thesis, it can be utilized for future projects. This means that there will be more time to study this concept extensively, rather than trying to find a fast and reliable solution to the existing problem. The thermal conductivity of aluminum is high, making it suitable for cases in which mechanical parts are subjected to high heat, however the strength of aluminum degrades rapidly at higher temperatures [16]. This means that from a heat transfer point of view, aluminum would be the ideal choice of material, however since the strength of the material degrades at higher temperatures which is the case for this project, this solution is not considered further. If this concept were to be implemented into the current or future projects, it is of great importance to carry out several studies to ensure that the quality of the machine would not diminish due to the use of aluminum. Aluminum when compared to steel is more expensive, hence cost calculations have to be done and verify if the increase in cost is worth it. The same thing applies to the second concept, that more in-depth FEM simulations have to be created to obtain reliable values for the resulting stresses. This is to ensure that such a solution would be possible to implement, without causing any problems.

6.4 Concept 3 Discussion and Future Work

The chosen dimensions for the beam reinforced solution in concept 3 are by no means optimized, hence further case studies have to be developed if Tetra Pak decides to pursue this concept. The dimensions of the beam has to be defined, alongside the method in which the beam is bonded onto the outer plate, for example through welding or bolting. Detailed case studies for the chosen method to bond the beam have to be performed. This can be done through performing simulations after the CAD-geometry is altered, or utilize existing standards to dimension the elements to ensure safety and quality. Cost calculations also have to be performed in combination with optimizing the solution, which should result in a safe, easy to implement and cost-effective solution. Extensive FEM simulations must be performed to ensure that no damage will occur to the production machine if this concept is implemented. This is not done in this thesis, since the main problem was to minimize the deformation and the overall geometries were simplified and often bonded together, resulting in unrealistic stress values.

7 Conclusion

The main findings of this thesis will be presented in this section.

7.1 Conclusions Regarding CFD and FEM Simulations

In this thesis, the steps taken to fully visualize a production flow are described in great detail. Numerous methods were used to optimize computational time and resources. Clear descriptions were written about how one can export data from CFD simulation software to then import them into FEM simulation software. This project clearly showcases the benefits of combining both CFD and FEM, whether it is to optimize production or to solve real-world problems in production equipment.

Numerous CFD and FEM simulations were performed, and documented in detail. The simulations will help understand ongoing problems related to side sealing equipment. The models and workflow developed in this thesis can be re-used to solve similar problems.

7.2 Conclusions Regarding the Generated Concepts

In this thesis, multiple concepts were developed and presented. The strength and weaknesses of the concepts were also discussed. The first concept, while very cost-effective, needs to be further studied, regrading the longevity of the machine, if one were to implement this concept. In addition, for the first concept, additional optimization of the thermal deformations that occur at the mid-section of the plate is also required. The second concept, in which the material was changed to aluminum instead of the typical stainless steel, shows great promise. The third concept, a beam reinforced one, is a cost-effective and easy to implement solution.

7.3 Recommendations for Tetra Pak

The main recommendation is to further develop the third concept, the beam reinforced one. This concept will increase the overall production of the side sealer. One would only need to apply an additional beam on the OS side. Making this concept very cost effective and since there will not be any material change, no studies regarding the strength of aluminum has to be made, since the beam can be of the same material as the outer plate. In addition, it is also clear where the beam has to be positioned, meaning that the company mainly has to decide on the dimensions of the beam and the choice of bonding technique. One can also calculate the costs of installing such a beam and optimize it so that the investment will be worth it long term. Lastly, stress calculations will also have to be performed to ensure the safety of the side sealer, when introducing the beam reinforced concept.

References

[1] Tetra Pak. *Heritage*. Available at https://www.tetrapak.com/about-tetra-pak/who-we-are/heritage. Accessed January 30, 2026. n.d.

[2] R. Bhaskaran and L. Collins. *Introduction to CFD Basics*. Available at https://dragonfly.tam.cornell.edu/teaching/mae5230-cfd-intro-notes.pdf. Accessed February 9, 2026. n.d.

[3] S. Pakravan. *Energy Convervation Energy*. Available at https://cfdland.com/energy-conservation-equation/. Accessed May 25, 2026. n.d.

[4] H. K. Versteeg and M. W. Malalasekera. *An Introduction to Computational Fluid Dynamics: The Finite Volume Method*. 2nd. Pearson Education Limited, 2007.

[5] CFD Online. *Finite Volume*. Available at https://www.cfd-online.com/Wiki/Finite_volume. Accessed May 26, 2026. n.d.

[6] Brilliant. *Finite Elements*. Available at https://brilliant.org/wiki/finite-elements/. Accessed February 10, 2026. n.d.

[7] S. N. Rosian and Y. S. Hoe. *Numerical Solutions of 2D Poisson Equation Using Finite Element Method and Finite Difference Method*. Available at https://science.utm.my/procscimath/wp-content/uploads/sites/605/2024/09/99-107-SITI-NURAISAH-BINTI-ROSLAN-A20SC0380.pdf. Accessed February 10, 2026. 2024.

[8] N. S. Ottosen and H. Petersson. *Introduction to the Finite Element Method*. Prentice-Hall, 1992.

[9] G. Laird. *Thermal-Stress Analysis*. Available at https://www.appliedcax.com/wp-content/uploads/Thermal-Stress-Analysis-with-Femap-and-NX-Nastran.pdf. Accessed May 26, 2026. 2015.

[10] Complete Era. *Tetrahedral vs Hexahedral Elements: Understanding the Differences*. Available at https://completeera.com/tetrahedral-vs-hexahedral-elements-understanding-the-differences/. Accessed May 26, 2026. n.d.

[11] M. Eriksson. *Fundamentals of a Methodology for Predictive Design Analysis*. Available at https://portal.research.lu.se/sv/publications/fundamentals-of-a-methodology-for-predictive-design-analysis/. Accessed April 14, 2026. 2015.

[12] Ansys. *Choosing a Turbulence model*. Available at https://ansyshelp.ansys.com/public/account/secured?returnurl=/Views/Secured/corp/v242/en/flu_ug/flu_ug_sec_turb_choosing.html. Accessed May 11, 2026. 2024.

[13] Ansys. *Prism Meshing*. Available at https://ansyshelp.ansys.com/public/account/secured?returnurl=/Views/Secured/corp/v242/en/icm_user/iuser_prismmesh.html. Accessed Mars 24, 2026. 2024.

[14] H. Karakes, E. Koyuncu, and G. Inalhan. *ITU tailless UAV design*. Available at https://www.researchgate.net/publication/257581521_ITU_tailless_UAV_design. Accessed Mars 13, 2026. 2012.

[15] Engineers Edge. *Thermal Conductivity of Common Metals, Alloys, and Materials*. Available at https://www.engineersedge.com/heat_transfer/thermal-conductivity-metals-alloys.htm. Accessed May 11, 2026. n.d.

[16] Aluminium Guide. *Aluminium at elevated temperatures*. Available at https://aluminium-guide.com/aluminium-elevated-temperatures/. Accessed May 11, 2026. n.d.